Unpublished Report of Findings

Dolomitization of the Middle Bakken Tight-oil Reservoir (Late Devonian – Early Mississippian, Williston Basin)

Maciej G. ŚLIWIŃSKI[1,2], B. Charlotte SCHREIBER[3], Akizumi ISHIDA[2,4], Erik HAROLDSON[5], Philipp P. KUHN[6], Susana SALAZAR-JARAMILLO[7], Adam C. DENNY[2,5], B. Davis BARNES[5], Michael J. SPICUZZA[2,5], Kouki KITAJIMA[2,5], Shanan E. PETERS[5] and John W. VALLEY[2,5]

[1] *Geological Consultant, Seattle, WA, 98034*
[2] *WiscSIMS, Department of Geoscience, University of Wisconsin-Madison, 1215 W. Dayton St., Madison, WI, 53706*
[3] *Department of Earth and Space Sciences, University of Washington, Seattle, WA, 98195*
[4] *Institute for Excellence in Higher Education, Tohoku University, Sendai, 980-8578, Japan*
[5] *Department of Geoscience, University of Wisconsin-Madison, 1215 W. Dayton St., Madison, WI, 53706*
[6] *Shell Global Solutions International, Rijswijk, Netherlands*
[7] *Departamento de Geociencias, Universidad Nacional de Colombia, Bogotá D.C., Colombia, 14490*

ACKNOWLEDGMENTS

The principle author (M.G. Śliwiński) extends his gratitude to J. W. Valley for providing the institutional scaffolding that supported much of this research study which was funded in large-part by the U.S. Department of Energy Office of Science, Office of Basic Energy Sciences, Chemical Sciences, Geosciences, and Biosciences Division (under award number DE-FG02-93ER14389). Supplementary financial backing was provided privately by the principle author and the generous support of Hanna M. and Tomasz A. Wietecha. The WiscSIMS Laboratory is financed in-part by the National Science Foundation of the United States (EAR-1355590, 1658823) and the University of Wisconsin-Madison. We warmly thank University of Wisconsin-Madison colleagues N. Kita (for guidance on SIMS methods), J. Kern (for SIMS instrument maintenance support), B. Hess (for masterful sample preparation), and John Fournelle and Bill Schneider (for assistance and guidance with EPMA and SEM). We also thank the kind folks at the North Dakota Geological Survey (Ed Murphy, Jeff Bader, Kent Hollands and Jonathan LaBonte) and the U.S.G.S. Core Research Facility for logistical guidance and assistance with core sampling, as well as Rick Sarg (Colorado School of Mines) and Kirt Campion (Marathon Oil Corporation) for helpful conversations along the way. We further express our gratitude to Han Machel (University of Alberta) for providing constructive guidance on an earlier version of this text. B.C. Schreiber's earlier foundational study (1981-1982) was carried out thanks to a year-long research project supported by Shell Houston, during a wide-ranging company review of diverse evaporite/carbonate lithologies chosen from various facies throughout the then-available outcrops and cored samples in North America and the United Kingdom.

ABSTRACT

A basic outline is established here for the dolomitization history of the mixed carbonate-clastic facies that comprise the middle Bakken tight-oil reservoir of the Williston Basin (Late Devonian – Early Mississippian). A mineralogical dataset compiled from sources in the public domain reveals a strong correspondence between the clay and dolomite content of middle Bakken facies and demonstrates how the presence and abundance of dolomite in the middle Bakken reservoir interval favorably influences matrix porosity and permeability.

Within the context of a well-constrained burial history and thermal evolution model recently developed for the Bakken Formation, pervasive dolomitization of the reservoir in the general vicinity of the depocenter occurred within ~30 m.y. of deposition and is restricted by the results of oxygen-isotope measurements ($\delta^{18}O$, performed *in-situ* by microanalytical means) and of fluid-inclusion microthermometry to temperatures < 70°C (< 160°F) and depths < 1.5 km (< 5,000 ft). The results of a mass-balance analysis indicate that the amount of dissolved Mg^{2+}

required to dolomitize the calcareous fraction of the reservoir rock matrix could have been sourced internally from clay-mineral reactions unfolding on a parallel diagenetic track if a modestly smectite-rich clay mineral assemblage is accepted as reasonable at the time of deposition. Thus, the amount of clay and of precursor calcium carbonate admixed with the silt / fine-sand fraction of middle Bakken facies appears to have exerted a dominant control over how much dolomite would eventually form during burial diagenesis.

1. INTRODUCTION

In the last decade, the Bakken Formation of the Williston Basin (Upper Devonian – Early Mississippian) has become the world's second-largest shale-oil producer (*e.g.*, Weijermars et al., 2017). The primary reservoir interval, informally referred to as the "middle Bakken member", is composed of variably dolomitized calcareous siltstones and fine-grained sandstones (*e.g.*, Meissner, 1978; Lefever et al., 1991) that were deposited along with some clay (~14 wt.% on average) in a shallow epicontinental seaway atop a regionally extensive ramp characterized by unusually broad facies belts (Peterhänsel et al., 2008; Egenhoff et al., 2011 and references therein). Horizontal drilling and hydraulic fracturing have been essential to production (*e.g.*, LeFever, 1992; Sonnenberg and Pramudito, 2009) given the low-porosity (4-8%) and low-permeability (0.01-0.001 mD) nature of the reservoir rock (*e.g.*, Sarg, 2012) and its rather limited thickness of no more than 26 meters (< 85 ft) (*e.g.*, Webster, 1984). The reservoir is charged by the surrounding Lower and Upper Bakken shale beds, which are regarded as world-class source rocks (*e.g.*, Gaswirth et al., 2013; Gaswirth and Marra, 2015).

Not surprisingly, the most severely dolomitized domains of this tight-oil reservoir are most porous and permeable (Sonnenberg and Pramudito, 2009). The purpose of this study was to contribute to a broader understanding of how a reservoir of this nature develops by outlining in time, temperature and burial-depth space the basic features of its dolomitization history. *When were favorable reservoir properties effectively established? What was the likely source(s) of dissolved Mg^{2+} and Fe^{2+} that facilitated the replacement of calcium carbonate ($CaCO_3$) by dolomite-ankerite ($Ca(Mg,Fe)(CO_3)_2$) in the reservoir facies package, and when and how did the alteration fluid(s) move through the system?*

Many distinctive styles of dolomitization have been recognized in ancient carbonate platform and ramp environments (*e.g.*, Warren, 2000; Machel, 2004). Continued interest in further understanding how this process unfolds is not merely an academic exercise, but also one that has considerable economic implications. Some 50% of the world's major petroleum reserves are hosted by carbonate rocks (*e.g.*, Ahlbrandt et al., 2005), about half of which contain abundant dolomite (*e.g.*, Zenger et al., 1980; Warren, 2000). In North America, approximately 80% of all carbonate-hosted oil and gas reservoirs have been dolomitized in some fashion (Zenger et al., 1980), making them more porous and permeable (on average) than their limestone equivalents (*e.g.*, Machel, 2004).

Dolomitization of marine sediments commonly occurs in multiple stages during burial (and any subsequent uplift; *e.g.*, Warren, 2000). Sediments undergoing compaction are progressively heated while the chemistry of the pore-fluid evolves due to reactions with unstable mineral phases and sedimentary organic matter (hydrologically closed-systems), but also in response to any infiltration(s) of extra-formational fluids (if the systems are, or at some point become, hydrologically open; *e.g.*, Hesse, 1999). Successive episodes of the dolomitization process can thus occur under distinctly different conditions, resulting in dolomite crystals that exhibit chemical and/or isotopic zonation. This includes, for example, core-to-rim variations in: 1) the abundance

of certain minor and trace elements (Mn, Sr, Ba, Pb, Na, B etc.) that tend to be characteristic of different sub-domains of the diagenetic realm (*e.g.*, Riciputi et al., 1994); 2) the amount of Fe^{2+} substituting for Mg^{2+} in the dolomite crystal structure; 3) radiogenic Sr-isotope signatures ($^{87}Sr/^{86}Sr$); and 4) variations in the stable isotope ratios of carbon and oxygen ($\delta^{13}C$ and $\delta^{18}O$, respectively), which were a central focus of the present study.

Isotopic studies of dolomite have traditionally made use of $\delta^{13}C$ signatures to aid in identifying the source(s) of dissolved inorganic carbon tapped during precipitation (Irwin et al., 1977; Barnes et al., 1999). Use of dolomite $\delta^{18}O$ signatures, on the other hand, has traditionally proven useful in broadly constraining (a) temperatures of precipitation or (b) in tracking the $\delta^{18}O$-evolution of the pore-fluid involved (through use of either theoretical or empirically-determined oxygen-isotope partitioning factors at different temperatures for the dolomite-water system at equilibrium; *e.g.*, Friedman and O'Neil, 1977; Horita, 2014 and references therein). More rigorous constraints require independent knowledge of either temperature or pore-fluid $\delta^{18}O$ (because both variables influence the $\delta^{18}O$ of dolomite), which – under favorable circumstances – can be gained through fluid inclusion microthermometry (*e.g.*, Goldstein, 2001; Machel, 1987) or clumped-isotope analysis (*e.g.*, Ghosh et al., 2006; Millán et al., 2016).

In this case, chemical zonation makes evident several distinct pulses of replacive micro-crystalline dolomite-ankerite growth in middle Bakken reservoir rock samples taken from deep basin cores. The conditions associated with each successive stage of the dolomitization process (temperature, depth, C-source(s) and pore-fluid $\delta^{18}O$) were here interpreted by pinning the results of fluid inclusion microthermometry and *in-situ* microanalysis of dolomite $\delta^{13}C$ and $\delta^{18}O$ to the existing framework of a well-constrained burial history and comprehensive thermal evolution model recently developed for the sedimentary fill of the Williston Basin (Kuhn et al., 2012). Until recently, resolving the isotopic evolution of micro-crystalline dolomite in fine-grained sedimentary rocks has been analytically untenable. Advances in isotope microanalysis by secondary ion mass spectrometry (SIMS), however, now allow for measurements of carbonate $\delta^{13}C$ and $\delta^{18}O$ to be performed *in-situ* from sample domains as small as 1-10 µm across (using either polished thin-sections or 25-mm diameter core plugs), with preservation of the petrographic context of the analyzed sample volume (Valley and Kita, 2009; Śliwiński et al., 2016a, 2016b, 2017).

The Williston Basin has a relatively simple and well-understood tectonic history (*e.g.*, Gerhard et al., 1982), and the wealth of available cores (a by-product of resource exploration) makes the Bakken Fm. an ideal natural laboratory for understanding not only in broad terms – but also in finer detail – how diagenetic processes unfold within carbonate-shale packages. One such process given considerable attention here is the evolution of pore-water $\delta^{18}O$ during burial (driven by water-rock interaction), which helps to establish first-order constraints that can be applied to the study of other Phanerozoic and more ancient basins where the burial and thermal history is only poorly known (*e.g.*, when inferring temperature/burial depth of sedimentary units from the $\delta^{18}O$ values of their mineral cements).

2. Samples and Methods

The samples chosen for this study were obtained from three cores recovered from northwestern North Dakota/northeastern Montana (wells A-C, Fig. 1). These samples represent a subset of the suite collected for study by Barnes (2017), which we examined using scanning electron microscopy (SEM; Hitachi S3400-N) and energy-dispersive x-ray spectrometry (EDS; ThermoFisher detector coupled to SEM) to locate regions of interest for *in-situ* $\delta^{13}C$ and $\delta^{18}O$

microanalysis of dolomite by secondary ion mass spectrometry (SIMS; CAMECA IMS-1280 at the WiscSIMS Laboratory, University of Wisconsin-Madison). Examination was performed on subsamples of core that were cast in epoxy (standard thin section-sized billets), polished to a 0.25-µm finish (using diamond suspensions) and coated with a thin layer of gold (~5 nm) to prevent charge build-up during imaging. See Śliwiński et al. (2016a,b,c) for an in-depth description of sample preparation and dolomite characterization by SIMS and later by electron probe microanalysis (EPMA of Ca, Mg, Fe, Mn and Sr concentrations using a CAMECA SX-51 at the Cameron Electron Microprobe Laboratory, University of Wisconsin-Madison).

2.1. In-situ isotope microanalysis of dolomite $\delta^{13}C$ and $\delta^{18}O$ by secondary ion mass spectrometry (SIMS)

In-situ $\delta^{13}C$ measurements by SIMS were performed using a 6-µm diameter spot-size with a precision of 0.6-1.2‰ (2SD, standard deviations), based on the spot-to-spot repeatability of replicate measurements (n = 8) of a drift monitor (end-member dolomite "UW6220" of Śliwiński et al., 2016a,b) which bracketed each set of approximately 10 sample analyses. A 10-µm spot was used to measure $\delta^{18}O$ with a precision of 0.3‰ (2SD; same drift monitor). An analysis of calibration curve residuals (matrix effect corrections as described in Śliwiński et al., 2016a,b) indicates an accuracy of 0.3‰ for both $\delta^{13}C$ and $\delta^{18}O$ in relation to the certified reference material NIST-19. The isotopic composition of analyzed sample domains is reported in terms of per mil (‰) deviations from the $^{13}C/^{12}C$ ratio in the Vienna Pee-Dee Belemnite ($^{13}C/^{12}C_{VPDB}$ = 0.0112372; Allison et al., 1995; Craig, 1957) and the $^{18}O/^{16}O$ ratio in Vienna Standard Mean Ocean Water ($^{18}O/^{16}O_{VSMOW}$ = 0.00200520; Baertschi, 1976) using conventional δ-notation.

2.2. Fluid inclusion microthermometry

Fluid inclusion analyses (microthermometry and salinity characterizations) were performed on doubly-polished thick sections (~80-µm thick, 0.05-µm finish) using a Linkam LMS600 heating-freezing stage mounted onto an Olympus BX50 microscope (University of Wisconsin-Madison). The system was calibrated using synthetic H_2O-CO_2 fluid inclusions at the melting temperature of CO_2 (-56.6°C / -69.9°F) and the dissociation point of clathrate (10°C / 50°F). Inclusions were classified using standard terminology and the criteria of Goldstein and Reynolds (1994) and Goldstein et al. (2003) for identifying fluid inclusion assemblages (FIAs). Fluid inclusion behavior was observed under 1000x magnification during cooling to a temperature of -185°C (-301°F) (near the limit of liquid N_2 freezing) and subsequent heating to 140°C (284°F). Despite difficulty with constraining the eutectic and hydrohalite melting temperatures, a H_2O-NaCl-$CaCl_2$-type fluid composition is interpreted based on the following observations and considerations (see also Skoreyko, 2017 who focuses on the hydrochemistry of the Bakken aquifer): 1) a reluctance of inclusions to freeze completely at temperatures near the liquid N_2 limit; 2) thawing behavior at a low of -63°C (-81.4°F); 3) final melting occurring in the presence of a vapor bubble at temperatures between -34 to -24°C; (-29.2 to -11.2°F) and 4) the general prevalence of H_2O-NaCl-$CaCl_2$-type fluids in sedimentary basins (*e.g.*, Goldstein, 2001). In all fluid inclusion assemblages, rapid growth and melting of the final melting phase was observed upon temperature cycling. Therefore, we interpret the final melting phase to be either ice or antarcticite, but not hydrohalite. The range in reported $CaCl_2$ and NaCl compositions accounts for all possible melting behaviors prior to final ice or antarcticite melting, as calculated using the numerical model and Microsoft® Excel©-based computer program developed by Steel-MacInnis et al., 2011. Isochores were calculated using MacFlinCor (Brown and Hagemann, 1994) and the

equations of Zhang and Frantz (1987). The prevailing temperature conditions under which each fluid inclusion assemblage developed were estimated from the intersection of isochores with a hydrostatic gradient calculated assuming a paleogeothermal gradient of 40°C/km (22°F/1000 ft, as in Pitman et al., 2001, after Gosnold, 1990), a constant surface temperature of 20°C (68°F) (as in Kuhn et al., 2012) and a fluid-pressure gradient of 105.2 bar/km (0.465 psi/ft; *e.g.*, see Fig. 5 in Meissner, 1978) (refer to Datashare 3).

2.3. Compilation of mineralogical data

A survey of existing x-ray diffraction (XRD) datasets was performed to determine how dolomite in the three Bakken members is distributed with depth of burial and how its abundance influences matrix porosity and permeability (middle Bakken only). A further objective was to examine whether there exists, on a regional-scale, any clear association between the clay and dolomite content of middle Bakken facies (from the perspective of clay diagenesis as a tenable source of dissolved Mg^{2+} and Fe^{2+} for replacive dolomite-ankerite growth). The intent was to frame within a broader, basin-scale context the results of pore-scale investigations of dolomite chemistry (as a proxy for the conditions under which it formed). The survey resulted in a compilation of data for 1318 samples collected over recent decades from 106 different cores recovered from burial depths ranging from approximately 0.5 to 3.5 km (1,650-11,500 ft). X-ray diffraction analyses and porosity/permeability measurements were performed primarily by commercial laboratories (*e.g.*, Weatherford Labs, Omni Labs, TerraTek, The Mineral Lab and others). These data were acquired primarily from well files available through the North Dakota Department of Mineral Resources – Oil and Gas Division (https://www.dmr.nd.gov/oilgas/) and the United States Geological Survey Core Research Center (https://my.usgs.gov/crcwc/). Further, a large portion of the data has been acquired as part of numerous theses and dissertations focused on the Bakken Fm. in the subsurface of North Dakota and Montana (*e.g.*, Grover, 1996; Smith, 1996; Alexandre, 2011; Almanza, 2011; Rolfs, 2015; Brennan, 2016; Listiono, 2016; Wescott, 2016; Nandy, 2018). This information was supplemented by data from the subsurface of southwestern Manitoba (Edwards, 1993; Karasinski, 2006) and southeastern Saskatchewan (Smith, 1996; Ferdous, 2001).

4. RESULTS

We begin with a basin-wide perspective by showing how dolomite is distributed with depth of burial and in relation to clay content, and how this in-turn influences measured porosity and permeability values of middle Bakken facies. We then turn to the results of pore-scale investigations of dolomite chemistry.

4.1. Basin-scale observations: Dolomite abundance vs. clays, facies, depth and reservoir properties

The abundance distribution of dolomite in middle Bakken interval is bimodal, with major and minor peaks at 13.5 and 33.5 wt.%, respectively (87% of all n = 877 datapoints fall between 0 and 30 wt.%), and a long tail extending to 75 wt.%. The surrounding shale beds are comparatively dolomite-poor (Figure 2): the abundance distribution is also bimodal, with major and minor peaks at 4.5 and 22 wt.% and a tail extending to 70 wt.%.

The clay distributions are approximately normal, with peaks at 14.5 wt.% in middle Bakken facies and 28.5 wt.% in the Bakken shales (Figure 2). The clay mineral assemblage is dominated by illite and mixed-layer illite/smectite (I/S), which are accompanied by subordinate amount of chlorite and kaolinite (Figure 3a; see also Pitman et al., 2001 and Sorensen et al., 2010). Illite and

mixed-layer I/S are typically present in sub-equal parts (Fig. 3b) and together account for 93% of the total assemblage (Fig. 2). The percentage of expandable (*i.e.*, smectitic) layers in mixed-layer I/S is limited to < 30%. Note that the overall character of the clay mineral assemblage in middle Bakken facies is indistinguishable from that of the Bakken shales (Figure 3a and b).

The distribution of dolomite in the middle Bakken and surrounding shale beds is plotted against present-day depth in Figure 2a. To a first-order, the dolomite content of samples from the realm of shallow burial (~0.5 to 1 km / 1,650 to 3,250 ft) does not appear to differ appreciably from what is observed in samples from greater depths (to 3.5 km / 11,500 ft; Fig. 4a). The dolomite content of the five major sedimentary facies of the middle Bakken member (facies A through F, *c.f.*, the classification established by the Bakken Consortium at the Colorado School of Mines; refer to Sarg, 2012) is shown in Figure 4b as a series of box charts stacked in ascending stratigraphic order. To a first-order, the abundance of dolomite increases up-section from an average low of ~10% (Facies A) to an average high of ~35% (Facies E). Second-order deviations from this general trend largely track changes in the average clay content of each facies (compare Figs. 4b-d). The clay content is a moderately strong predictor of dolomite content (Fig. 4d; Pearson's r = 0.780).

Plotting the porosity of middle Bakken reservoir rock samples against present-day depth shows values near 15% at ~1 km (3,250 ft) of burial and a consistent range of values effectively between 1 and 10% in the depth interval between ~2.5 and ~3.5 km (8,200 to 11,500 ft; Figure 4e). Note that here the data points are color-coded according to the amount of dolomite present in the carbonate fraction of each sample (wt.% dolomite / wt.% (calcite + dolomite), here abbreviated as 'f_{Dol}' with values falling between 0 and 1), revealing a gradient between low porosity (~1-3%) and a low degree of dolomitization ($f_{Dol} < 0.2$) on one end, and relatively high porosity (~8-10%) and a high degree of dolomitization ($f_{Dol} > 0.8$) on the other. This is made more apparent when porosity is plotted directly against fractional dolomitization as shown in Figure 4f, where the data are instead color-coded according to present-day depth. On a facies-specific basis, the porosity is: 1) highest in Facies B, C, and E (mode at ~6%), 2) intermediate in Facies A (mode at ~4%), and 3) lowest in Facies D (mode at ~2%) (see Fig. 4g). Finally, the permeability of the reservoir rock is highest where it is most extensively dolomitized (Fig. 4h).

4.2. Core-scale observations: Dolomite distribution in Well A

Shown in Figure 5a is the stratigraphic profile of one the wells from which samples were collected for evaluating the isotopic evolution of dolomite by *in-situ* means (Well A, Fig. 1). The total carbonate content (calcite + dolomite) throughout the middle Bakken interval shows an apparent stratigraphic baseline value near 25% (Fig. 5b). Moving up-section through Facies B, C and D, the carbonate content remains at baseline (no data for Facies A). It then increases markedly in the upper third of the profile to a high near 40% (Facies E) before returning to baseline (Facies F). Dolomitization of precursor calcium carbonate is pervasive throughout the section (f_{Dol} generally > 0.8, but no smaller than ~0.6; Fig. 5c). Shown for reference is the generally low (<15%) carbonate content of the Upper and Lower Bakken shales (where dolomite again dominates the carbonate fraction).

4.3. Pore-scale observations: Chemical and isotopic composition of dolomite-ankerite

We observed up to four distinct generations of dolomite in the facies of the middle Bakken reservoir interval on the basis of consistent concentric chemical zoning patterns observed in crystals via BSE-imaging (Fig. 6). Each generation is the product of a particular "stage" or episode of the dolomitization process. To a first-order, the core-to-rim composition evolves unidirectionally along the dolomite-ankerite join of the Ca-Mg-Fe carbonate ternary, beginning

with non-ferroan dolomite and ending with ankerite containing up to 20% $FeCO_3$ end-member (Fig. 7). The Fe-richness of dolomite can also be discussed in terms of the molar Fe/(Mg+Fe) ratio, or "Fe#" (*e.g.*, Chang et al., 1998). Here, dolomite is referred to as: i) "non-ferroan" for ratios between 0 and 0.05, ii) ferroan for ratios between 0.05 and 0.2, and iii) as ankerite for ratios > 0.2.

Dolomite crystal cores (Stage I) are non-ferroan with a sub- to euhedral morphology and typically measure < 50-µm across ("medium crystal size'' following the classification of Lucia, 1995; Figs. 6a-b, 7). These are mantled by ferroan rims (Stage II) (Figs. 6a-b, 7). Both stages are volumetrically sub-equal and result in a planer-e fabric (Sibley and Gregg, 1987) where the total dolomite abundance is high (up to ~50%; Fig. 4a). In considering data from all sampled localities collectively, both dolomite Stage I and II respectively show the following average $\delta^{18}O$ values (± 2SD): 25.6‰ (±2.3, VSMOW) and 26.0‰ (±2.6, VSMOW). The corresponding average $\delta^{13}C$ values (± 2SD) are as follows: 0.3‰ (±1.9, VPDB) and -1.4‰ (±2.5, VPDB) (see Fig. 8a and Table 1; the complete SIMS and EPMA datasets are provided in Datashare 1, whereas supporting petrographic documentation of all analyzed sample domains can be found in Datashare 2).

Iron-rich (ankeritic) overgrowths (Stages III and IV) are encountered primarily in fractures, vugs and post-compaction pore-space (Fig. 6c-h). They measure up to several hundred micrometers across and are collectively comprised of up to six concentric zones (3 each, see Fig. 6f) layered around the two-stage crystals that grew earlier during the main dolomitization episode. All spatially-coupled $\delta^{13}C$ and $\delta^{18}O$ measurements (Fig. 8a) from several crystals probed within the mineralized fracture of sample A in well A (Figs. 1, 5e, Table 1) were projected onto the representative transect line shown in Figure 6f (each data pair plotted at the mid-point of the appropriate compositional zone). The resulting composite transect (Fig. 8b) shows: 1) a first-order core-to-rim decrease of $\delta^{13}C$ and $\delta^{18}O$ values (by approx. 4 and 9‰ in the case of $\delta^{18}O$ and $\delta^{13}C$, respectively); and 2) a strong covariance of $\delta^{13}C$ and $\delta^{18}O$ values between Stages II and IVa of crystal growth.

4.4. Results of fluid inclusion microthermometry

Fracture-filling calcite cement in Sample A of Well A (sampled fracture shown in Fig. 5e, well location in Fig. 1) contains assemblages of two-phase (liquid-vapor) aqueous fluid inclusions entrapped along what appear to be crystal growth zones (refer to supporting petrographic documentation in Datashare 3). Four such assemblages were analyzed within the crystal shown in Figure 6e, located near the center of the vein. The innermost of the analyzed assemblages indicates growth entrapment at 67-76°C (153-169°F), whereas the next three yielded entrapment temperatures of 82-84°C (180-183°F), 77-83°C (171-181°F) and 89-101°C (192-214°F) (Table 2). One additional lone assemblage was analyzed in a crystal situated nearer the vein wall (see Datashare 3), which provided a temperature constraint of 59-70°C (138-158°F) and presumably reflects upon the prevailing conditions during the early stages of vein-filling calcite growth. This vein type falls in the category of what Sonnenberg et al. (2011) described in the Bakken Fm. as "tectonic extension fractures." To date, we have examined the mineralogy of this fracture-type at multiple localities across the basin (via SEM and EDS analysis) and noted that the layering pattern of mineral precipitates points to several stages of opening/widening and in-filling, initially by calcite (+/- pyrite) and later by anhydrite. The calcite can be replaced by ferroan dolomite and ankerite to a moderate degree. As in the example shown in Figure 6e, both calcite and dolomite can have a corroded appearance due to a dissolution event of some degree that occurred prior to anhydrite cementation (calcite in this instance was far more extensively affected than dolomite, many crystals of which remain only minimally blemished).

Assemblages of two-phase aqueous fluid inclusions were also identified within fracture-hosted dolomite-ankerite crystals (in growth Stages II and IIIa; Sample A, Well A, see Fig. 5e). Within fractures, Stages II, III and IV were observed: 1) sequentially enveloping the faces of Stage II crystals exposed along fracture walls and 2) floating throughout the vein body, surrounded by calcite and anhydrite (in both cases crystal faces are well-developed). The same general chemical zoning pattern and isotopic characteristics are exhibited by dolomite-ankerite crystals in fractures and those lining the pore network of the host-rock (crystals differ primarily in size; Fig. 9). Two fluid inclusion assemblages (FIAs) were analyzed. The first is confined to the crystal growth-band of Stage IIIa (Fig. 6h). Inclusions measuring ~1-10 µm in length are preferentially oriented in the direction of crystal growth (Datashare 3). The analyzed assemblage indicates growth entrapment at 116-125°C (241-257°F) and meets the criteria outlined by Goldstein (2001) for a fluid inclusion assemblage to be regarded as primary (*e.g.*, aqueous inclusions of variable size and shape – however with vapor bubbles of similar volume – oriented in the direction of crystal growth and confined to a readily-identifiable growth zone, 90% of which yield homogenization temperatures within a range of 10-15°C (20-30°F). The second FIA is confined to Stage II, which appears to have been affected by recrystallization. This is first and foremost evident in BSE-imagery which reveals a mottled and pitted compositional "texture", and, perhaps most importantly, the presence of small (< 5-µm) anhydrite-filled cavities (Fig. 6h, Datashare 3). Preferential alteration of the crystal interior is expected if the initial stages of crystal growth occurred at the relatively low temperatures of the shallow burial environment (where conditions favor metastable dolomite varieties; *e.g.*, Carpenter, 1980; Warren, 2000; Gregg et al., 2015) before being transported deeper into the sediment pile. Although a relatively narrow range of homogenization temperatures was observed, we interpret re-equilibration of this FIA, meaning no reliable estimate of trapping temperature can be made.

5. DISCUSSION AND INTERPRETATIONS

The discussion that follows is focused around the following three questions: 1) *When did the middle Bakken reservoir interval become effectively dolomitized (or, more specifically, when did the volumetrically-significant episodes of the dolomitization process occur?);* 2) *How did the O-isotope composition of the pore-fluid evolve across all stages of dolomite-ankerite crystal growth?* and 3) *What was the predominant source of dissolved Mg and Fe ions that enabled the growth of dolomite-ankerite at the expense of the calcareous fraction of the mixed carbonate-clastic facies of the reservoir interval?*

5.1. *Inferred timing of pervasive dolomitization (Stages I and II)*

The bulk of the dolomite volume encountered in the middle Bakken interval across the expanse of the Williston Basin, in shallow (~0.5 to 1 km / 1,650 to 3,250 ft) and deep (~3.5 km / 11,500 ft) burial environments alike, appears to be the product of only two distinct episodes of crystal growth (*e.g.*, Ferdous, 2001; Karasinski, 2006; Alexandre, 2011; Brodie, 2016; Staruiala, 2016; Brodie et al., 2018). The chemo-isotopic properties of both Stage I and II dolomite at the sampled deep-well localities of this study in NW North Dakota and NE Montana (3.0-3.3 km / 9,850 to 10,850 ft depth interval; Figs. 1, 7, 8, Table 1) bear a strong resemblance to those determined by broadly-analogous *in-situ* methods for the two-stage dolomite encountered at shallower depths across much of southeastern Saskatchewan (where the Bakken presently resides at subsurface depths of ~0.5-2.5 km / 1,650 to 8,200 ft; this data from Staruiala (2016) is coplotted for comparison in Fig. 7 and 8a herein, whereas the corresponding well locations are shown in Fig.

1). One question that thus emerged is whether dolomite Stages I and II are present in any of the shallowest Bakken cores situated on the basin's eastern margin in North Dakota, as knowledge of this would allow for placing upper limits on the depth, temperature and timing of dolomitization based on the independently-constrained burial and thermal history model created by Kuhn et al. (2012; which does not cover the Canadian expanse of the Williston Basin). To date, we've examined one such cored locality (Well D in Fig. 1) where the unit was buried no more than ~1 km (~3,250 ft) and heated to an estimated maximum of 70°C (160°F; Fig. 10). Dolomite Stages I and II are well-developed at this basin-margin location (Fig. 6a), whereas the Stage III and IV ankerite rims observed in deep basin cores appear absent. An examination of the burial and thermal history reconstruction for the central Williston Basin suggests that a temperature of ~70°C (~160°F) was attained as early as the Late Mississippian (~325 Ma; see Fig. 6 in Kuhn et al., 2012 and Fig. 8b herein, showing a reconstruction specific to Well A of Fig. 1). We thus infer that within the general vicinity of the depocenter, the two dolomite generations that are most volumetrically significant (Stages I and II) from the perspective of influencing the reservoir-quality of middle Bakken facies likely developed well within ~30 million years after deposition.

The compilation of mineralogical data for the middle Bakken member from across the basin reveals no significant increase in dolomite abundance with depth beyond approximately 1 km of burial (~1,650 ft; Fig. 4a), attesting to reservoir dolomitization being effectively complete during the early stages of the burial history. The early establishment of a pore-space supporting framework composed of dolomite, abundant silt and fine sand-sized quartz grains likely restricted the compactional potential of the lime mud that initially comprised up to approximately one-half of the sediment volume, allowing for porosity and permeability preservation (broadly analogous to the circumstances and process described by Weyl, 1960). Regardless of facies and subsurface depth in the interval between ~2.5 and 3.5 km (8,200 to 11,500 ft), measured reservoir porosity values are highest where the extent of dolomitization of precursor calcium carbonate is greatest, with permeability generally following suit (Fig. 4e-h).

5.2. Pore-fluid $\delta^{18}O$ during dolomitization Stages I and II

Per accepted standards, the evolution of the pore-fluid's oxygen-isotope composition ($\delta^{18}O$) is discussed here relative to the VSMOW isotope reference scale. Thus, the $\delta^{18}O$ of dolomite is also discussed here relative to VSMOW, with equivalent VPDB values shown parenthetically (see also Table 1). For conversion between the two reference scales, see Coplen et al. (1983), for example.

The average $\delta^{18}O$ value determined for Stage II dolomite from all three cored localities (26.0 ± 2.6‰ VSMOW / -4.8 ± 2.6 VPDB) suggests the involvement of a +2‰ $\delta^{18}O$ pore-fluid if precipitation occurred at the above-proposed maximum possible temperature of 70°C (160°F; range: -0.5 to +4.5‰ VSMOW; calculated using the dolomite-water equilibrium isotope fractionation relation of Horita, 2014). Driven by gradual water-rock interaction, this would amount to an average ^{18}O-enrichment of +4‰ relative to marine waters of Late Devonian low-latitude epicontinental seaways, with an estimated $\delta^{18}O$ of -1 to -3‰ VSMOW. This constraint on the starting point of the pore-fluid's $\delta^{18}O$-evolution stems from conventional isotope studies of well-preserved calcitic brachiopods (van Geldern et al., 2006) and reefal cements from around the globe (*e.g.*, Carpenter and Lohmann, 1989; Hurley and Lohmann, 1989) and an estimated precipitation temperature of 25-30°C (77-86°F; based on studies of conodont apatite $\delta^{18}O$, which serves as a seawater temperature proxy; *e.g.*, Kaiser et al., 2006; Longinelli and Nuti, 1973; Luz et al., 1984). The isotopic composition of calcite that occurs as early pre-compaction cement in

un-dolomitized sediment lenses (cm-m scale; $\delta^{18}O$ = 25.7 to 28.3‰ VSMOW; Brennan 2016) within the middle Bakken interval offers an additional regional constraint on the $\delta^{18}O$ of contemporaneous seawater. Assuming precipitation at 25-30°C (77-86°F) suggests the involvement of waters with an average $\delta^{18}O$ of -1‰ (range: -3 to +0.5‰ VSMOW; calculated using the calcite-water equilibrium fractionation relation reported in (Friedman and O'Neil, 1977), falling in agreement with global estimates.

5.3. Pore-fluid $\delta^{18}O$ during dolomitization Stages III and IV

We now turn to examining the isotopic record of Stage III & IV ankeritic crystal rims, the thickest of which occur in vugs and fractures (100-µm scale crystals; Fig. 6c-h). One obvious question, however, is whether the isotopic record of fracture-filling dolomite-ankerite is representative of the temperature and pore-fluid conditions to which the host-rock was subjected throughout progressive burial and heating. A zone-by-zone comparison of chemo-isotopic properties (Fe-content, $\delta^{13}C$ and $\delta^{18}O$) of fracture-filling *vs.* rock-matrix dolomite shows a near 1:1 correspondence, suggesting that a similar fluid was sampled during growth (see Fig. 9). Thus, it is here that the most extensive and readily analyzable record of pore-fluid evolution appears to be preserved from the later stages of the burial history. Analogous rims mantle earlier dolomite crystal faces once-exposed to post-compaction pore-space within the host-rock itself, although most zones in the sequence are generally too thin to accommodate a 6-µm diameter $\delta^{13}C$ analysis spot (some portion of the outermost subzones can also be absent due to limited space).

Fluid inclusion microthermometry indicates a temperature of 116-125°C (241-257°F) during Stage IIIa of crystal growth, whereas microanalysis of dolomite $\delta^{18}O$ yielded values of 22.2 to 23.8‰ VSMOW (-8.4 to -6.9‰ VPDB; Table 1, sample A, Well A) within this relatively narrow compositional zone that measures only ~15-20-µm across. Together, these two pieces of information allow for a near-direct appraisal of pore-fluid $\delta^{18}O$ at this stage of the dolomitization process by use of a temperature-dependent equilibrium isotope fractionation relation for the dolomite-water system. Using the recent empirically constrained relation of Horita (2014) indicates the involvement of an evolved fluid with an average $\delta^{18}O$ of +6‰ (VSMOW; range: 4.5 to 7‰), which amounts to an ^{18}O-enrichment of ~8‰ relative to Late Devonian seawater in the shallow tropics (Fig. 11). Within the framework of the burial and thermal history model for the Bakken Fm. proposed by Kuhn et al. (2012), the precipitation of Stage IIIa can be firmly anchored in time-temperature and depth space. At the well site in question (Well A, Fig. 1), the unit would have experienced the temperatures deduced from the properties of entrapped fluid inclusions some 50 million years ago (Late Cretaceous – Early Paleocene time) while residing at maximum burial (~3 km / 9,850 ft; Fig. 10b).

It is interesting to note that present-day reservoir brines in the Midale area of Saskatchewan, located some 100 km away from the well-site in question (Well A, see Fig. 1), yielded $\delta^{18}O$ values of +5.0 to 5.6‰ (Rostron and Holmden, 2000). There, the Bakken reservoir resides at a shallower depth of ~2 km (6,550 ft) (*e.g.*, Christopher, 1961; Kohlruss and Nickel, 2013) and was likely never heated beyond 110-115°C (230-239°F; Fig. 1). As such, the pore-fluid may still be under-evolved in terms of $\delta^{18}O$ compared to deeper settings in the basin, where the diagenetic potential was more fully expressed. More generally, the $\delta^{18}O$ of Bakken Fm. brines from undisclosed wells in North Dakota and Montana fall between +4.5 and +7.5‰ (VSMOW; see Fig. 6 in Peterman and Thamke, 2016).

Without a second anchor-point, however, we can only speculate about the conditions (temperature and pore-fluid $\delta^{18}O$) under which all subsequent dolomite-ankerite bands developed

(Stages IIIb-c, IVa-c). Given that precipitation rates increase with temperature (*e.g.*, review of Gregg et al., 2015), the time required for the formation of Stage III and IV rims at temperatures >130°C (265°F) was likely minor in comparison to the length of time required for Stage I and II dolomite growth at <70°C (160°F). Thus, the conditions determined for Stage IIIa may well be representative for all later stages of rim formation. This is supported by the following consideration: if we use the high-end pore-fluid $\delta^{18}O$ value from Stage IIIa (+7‰ VSMOW), we obtain a precipitation temperature estimate of 130°C (265°F) for the very outmost band (Stage IVc; average $\delta^{18}O$ of 23.5‰ VSMOW) of the volumetrically minor ankeritic overgrowths that mantle, where space permits, the pervasive micro-dolomite that established the reservoir properties of the middle Bakken interval during the early stages of burial. This estimate is essentially in agreement with the maximum diagenetic temperature predicted for the Bakken Fm. at the well site in question (130-140°C / 265-285°F) by the thermal evolution model of Kuhn et al. (2012; Well A, Fig. 1).

5.4. *Dissolved inorganic carbon source(s) tapped during dolomitization*

Well-preserved, early marine calcite cements in Late Devonian reefs from around the globe allow for estimating the $\delta^{13}C$ of the dissolved inorganic carbon (DIC) pool of low-latitude epicontinental seaways (*e.g.*, Hurley and Lohmann, 1989). These cements show an average $\delta^{13}C$ value of 2.5‰ (± 1.0, VPDB). Assuming precipitation at 25-30°C (77-86°F; refer to discussion above) yields a $\delta^{13}C_{DIC}$ range of -6 to -9‰ (average = -7.5‰ VPDB; using the equilibrium fractionation relation of (Bottinga, 1968; Friedman and O'Neil, 1977).

A hypothetical dolomite precipitated at 40°C (104°F) from a parent-fluid of this composition would take on $\delta^{13}C$ values of +0.5 to +3.5‰ (VPDB; equilibrium fractionation relation of Horita, 2014). This scenario reproduces the general range of $\delta^{13}C$ values measured from Stage I dolomite of the middle Bakken reservoir across the expanse of the Williston Basin (Fig. 8a). In the case of precipitation at 70°C (160°F), dolomite would take on $\delta^{13}C$ values of -2.5 to +0.5‰ (VPDB). This scenario in-turn reproduces the general range of $\delta^{13}C$ values measured from Stage II dolomite (Fig. 8a). Thus, seawater is considered to have been the predominant DIC source tapped – directly or indirectly – during the early stages of reservoir dolomitization (indirect tapping *sensu* dolomite inheriting, in large part, its $\delta^{13}C$ signature from precursor $CaCO_3$ precipitated in equilibrium with seawater).

The isotopic composition of the dissolved inorganic carbon-pool apparently remained rock-buffered into Stage IIIa of dolomite-ankerite growth at the time of maximum burial and heating (although prior to hydrocarbon migration). With the temperature of precipitation constrained via fluid inclusion analysis (117-127°C / 243-261°F), measurements of Stage IIIa dolomite $\delta^{13}C$ values (-4.5‰ VPDB; Table 1) allow for constraining directly the $\delta^{13}C$ of the DIC pool at this stage of the alteration process. Again using the equilibrium relation established by Horita (2014) for the dolomite-water system indicates the involvement of a DIC pool with an average $\delta^{13}C$ of -7.5‰ (VPDB; *i.e.*, largely unmodified at this stage by isotopically-light carbon derived from organic maturation). This same conclusion seems to hold for the remainder of the dolomite growth history (Fig. 8b).

6. *Interpretation*

We offer the following interpretation of the data as a contribution towards a better understanding of the predominant mechanism/process by which the rock volume of the middle Bakken tight-oil reservoir became dolomitized. The interpretation is more broadly applicable as a

starting point or framework for an evaluation of the diagenetic evolution of similar unconventional reservoir types elsewhere.

In the present case, dolomite has replaced – anywhere from partially to pervasively – the calcareous fraction of the original sediment (largely precursor lime mud). This post-depositional alteration has favorably affected the porosity and permeability of the rock matrix (excluding fracture permeability, the controls of which have been previously discussed in the literature; *e.g.*, see Sarg, 2012 and Pitman et al., 2001). The values of both properties increase in concert with dolomite content, which in-turn covaries with the concentration of clays and of precursor calcium carbonate (for example on the facies-scale, but also more generally – see Fig. 4b-d).

As we will elaborate below, the data has led us to suspect that dolomitization of the Bakken Fm. was driven in large-part by fluid-flow related initially to sediment compaction and later to clay dehydration reactions, with the requisite amount of Mg^{2+} therefore supplied by two internal reservoirs: 1) the volume of pore-water expelled from the middle Bakken interval and the shale beds that enclose it; and 2) the clay mineral assemblage itself (*c.f.* the arguments of (Shields and Brady, 1995) high-Mg calcite is not considered a major Mg-source in the present case). At the same time, however, we do not exclude the possibility that some portion of the total dolomite volume along the basin margin could also be ascribed to local, syn-sedimentary evaporative brine reflux (note, for example, the comparatively high dolomite content of the middle Bakken in shallow wells from SW Manitoba in Fig. 4a). Fluids expelled from compacting and dehydrating shale beds can be sufficiently enriched in dissolved Mg^{2+} and Fe^{2+} to become an effective agent for dolomitizing large swaths of adjacent carbonate-rich strata through which they flow (Machel and Mountjoy, 1987, 1986; Machel and Anderson, 1989 and references therein). It is during the first kilometer of burial that the volume of pore-water expelled from compacting clays and shales is largest (Fig. 12; initial porosity reduction from ~70-80 to 30%), falling off exponentially thereafter until clay mineral dehydration reactions begin at ~80°C (~175°F) (Powers, 1967; Burst, 1969; Perry and Hower, 1970, 1972; Hower et al., 1976; Galloway, 1984; Chamley, 1989). The clay dehydration process commonly involves the step-wise illitization of smectite-group clays, which is accompanied by the release of volumetrically significant quantities of dissolved Si^{4+}, Mg^{2+} and Fe^{2+} into the pore-fluid (+/- subordinate quantities of other ions; *e.g.*, see Boles and Franks, 1979; Foscolos et al., 1990; Milliken, 2003) and continues until the sediment package attains a temperature in the range of ~130°C (265°F; the depth interval over which this process unfolds depends on the geothermal gradient; see Fig. 12 and, *e.g.*, Burst, 1969; Perry and Hower, 1972; Boles and Franks, 1979; Foscolos et al., 1990; Whitney and Northrop, 1988). During the 2nd and 3rd stages of interlayer water loss and ion expulsion, "the amount of water in movement should constitute 10-15% of the compacted bulk volume. This movement is the most significant fluid displacement subsequent to the initial pore-water drainage, and is capable of redistributing mobile subsurface components" (Burst, 1969, pg. 80).

We now turn to assessing the feasibility of such a dolomitization scenario by first considering whether the clay mineral assemblage could have been smectite-rich at the time of deposition (and consequently a large, tenable source of dissolved Mg^{2+} for dolomitization) and later via a Mg mass-balance analysis; the latter provides an estimate of how much Mg^{2+} may have initially resided in the compaction water volume and clay mineral fraction associated with each of the three Bakken members.

6.1. *The Bakken clay mineral assemblage as a Mg-source*

We begin with the question: *What was the probable nature of the Bakken clay mineral assemblage at the time of deposition?* Most of the available clay speciation data that we were able to acquire for this study is associated with wells where temperatures at maximum burial reached ~120-165°C (250-330°F; Fig. 1). In these wells, illite is reported as the predominant clay type (accompanied by subordinate amounts of chlorite; *e.g.,* Pitman et al., 2001; Sorensen et al., 2010), resulting in what seems to be the prevailing view that it is mostly detrital in origin (*e.g.* Pitman et al., 2001; Wilson et al., 2016). However, a predominance of illite is also what would be expected for an initially smectite-rich clay assemblage subjected to such temperatures during burial (*e.g.,*Boles and Franks, 1979; Chamley, 1989; Wilkinson et al., 1992; Milliken, 2003). Indeed, the conversion of smectite to illite (mica) or chlorite is one of the primary reactions of marine diagenesis (*e.g.,* Borchardt, 1989 and Chamley, 1989 and references therein). One study (Grover, 1996, pg. 132) notes that "samples of shallow clay-rich limestone and middle Bakken siltstone have smectitic clays, indicating that smectite was being deposited in the basin" (see also Karasinki, 2006, who reports smectite-bearing clay assemblages in the Bakken from wells in southwestern Manitoba, where the unit resides in the shallow subsurface (< 1 km / 3,250 ft). Little more seems to be known, however, about the exact nature of the clay mineral assemblage in wells from the shallow basin margin where the source rocks remain immature and where the clay assemblage would be least altered by burial diagenesis.

However, certain broad inferences can be made about the initial compositional characteristics of the clay mineral assemblage deposited in the Bakken sea by considering what is known about the climatic conditions, soil types, and floras of the tropics during Late Devonian – Early Mississippian time. This stems from the reality that the mineralogical character of clay assemblages carried by rivers and coastal runoff to marine depositional environments "chiefly reflect[s] the composition of soils in the drainage basin" (Chamley, 1989, pg 66). The overall character of the soils in-turn depends strongly on the "intensity of weathering, and especially of hydrolysis [*i.e.,* chemical weathering], in the land masses adjacent to sedimentary basins (Chamley, 1989, pg 455).

In terms of Late Devonian – Early Mississippian paleogeography, the Williston Basin province was a shallow (< 200 m water depth), semi-restricted epicontinental embayment situated at near-equatorial latitudes (5-10°N) along the southwestern coast of Laurentia (North America) (*e.g.,* Scottese and McKerrow, 1990; see also Domeier and Torsvik, 2014). The province is regarded as a sub-domain of the Western Canada Sedimentary Basin (WCSB) (*e.g.,* Kent and Christopher, 1994) and its vast expanse of epeiric environments, which included some of the largest known reef complexes and carbonate platforms of the Phanerozoic (*e.g.,* see paleogeographic depictions in Smith and Bustin, 1998, Scottese and McKerrow, 1990; Hauck et al., 2017). Dispersal patterns of land-derived clastics (quartz, feldspars, clays, etc.) are largely consistent with progressive infilling of the WCSB from the north-northeast towards the south-southwest (Stoakes, 1980; Wendte and Uyeno, 2005). The clastic fraction of the sediment fill was derived primarily from weathering of the distant Innuitian-Ellesmerian Orogen of Arctic Canada to the north, and of the Laurentian continental interior to the east / northeast (the lowlands of the Canadian Shield) (*e.g.,* Hauck et al., 2017; Ibrahim, 2014; Stoakes, 1980). Discernable eolian contributions have also been reported (*e.g.,* Whalen and Day, 2008).

Following a prolonged period of largely global greenhouse conditions that persisted for nearly 80 million years, the Earth's climate in the terminal Devonian was in transition to the general icehouse conditions that prevailed during much of the Carboniferous. In the low-latitudes, this unfolded as a series of relatively rapid fluctuations (100 k.y. time scales) between broadly

warm/humid and temperate/sub-arid conditions (Kaiser et al., 2016; Streel et al., 2000; Smith and Bustin, 1998 and further references therein). More generally, the conditions can be described as more savanna-like than ever-wet (Streel et al., 2000), with alternating dry and wet seasons imposing a discontinuous weathering regime on the land surface. Smectites are abundant in the soil-types that develop under such conditions atop a diversity of parent rock types, and, depending on the intensity of hydrolysis (with conditions of moderate leaching generally optimal), can comprise 60-90% of the clay mineral assemblage in the upper soil horizons in temperate-warm and dry tropical areas of the globe (*e.g.*, Ahmad, 1983; Allen and Fanning, 1983; Chamley, 1989). The development of such soils, known as vertisols or black earths, became increasingly common during the Late Devonian (385.3 – 359.2 Ma), as the continents became forested by deeply-rooted vegetation for the first time in our planet's evolutionary journey. As primordial forests swiftly colonized land surfaces from the tropics to the boreal latitudes (*e.g.*, Streel et al., 2000), the character of continental weathering changed fundamentally (*e.g.*, Algeo et al., 1995, 2001; Algeo and Scheckler, 1998, 2010 and references therein). Net increases in the annual production of organic-acids in terrestrial environments likely elevated by several orders of magnitude the baseline efficiency of chemical weathering, and broadened considerably the range of environments favorable to smectite formation. It is during the Late-Devonian – Early-Carboniferous time-frame that deeply-weathered soil profiles, along with apparent analogous of all the dominant soil-types that are characteristic of modern swamps and forests, first appear in abundance in the geological record (*e.g.*, Retallack, 1986; Mora et al., 1991; Algeo et al., 2001).

Based on these considerations, an initially smectite-rich clay mineral assemblage thus seems most probable at the time of Bakken deposition. The question then becomes one of deciding*: What degree of initial smectite-richness is appropriate for the following mass balance analysis?* The ratio of smectite to illite in the clay fraction of surficial sediments accumulating in today's low-latitude ocean basins provides one constraint: on average, the value of this ratio in the most smectite-rich clay assemblages does not exceed ~0.65 (*e.g.*, see Table 8.1 and discussion in Chamley, 1989). Using this value as an approximation in the mass balance analysis (*i.e.*, assuming that 65% of the present-day illite content was initially smectite) would likely results in the most conservative estimate of the clay mineral-hosted Mg-reservoir size given that in its coolest phase, the climate of the low-latitudes during Bakken deposition (the middle Bakken regressive facies package) may have been somewhat warmer relative to conditions today, and hence more conducive to smectite formation through enhanced chemical weathering.

6.2. *Mg mass-balance analysis*

The size of the internal Mg-reservoirs for the Bakken Fm. (*i.e.*, the compaction water volume and clay fraction of each member) was estimated using as a guide the considerations and general problem setup of Machel and Anderson (1989, pg. 907). The characteristics of this rock unit most relevant to the following analysis are best known from the subsurface of North Dakota (*i.e.*, the spatial geometry, mineralogy, average rock density and porosity values). Estimates of rock volume, subsurface area and average thickness were thus only made for the North Dakotan portion of the Williston Basin (Table 3). These were based on the isopach maps of LeFever (2008) (estimated made using ImageJ image-analysis software; Schneider et al., 2012).

The mass of Mg^{2+} that has been diagenetically sequestered by dolomite in the middle Bakken member and the under- and overlying shale beds was calculated by converting porosity-adjusted rock volumes to rock mass (via average density, calculated based on mineralogical data obtained by x-ray diffraction analysis) and multiplying through by the average mass fraction of

dolomite and by the mass fraction of Mg in the structural formula of end-member dolomite (Table 3).

The total amount of dissolved Mg^{2+} that passed through the system during compactional dewatering of the sediments was estimated by assuming: 1) a porosity loss of 65% for the upper and lower Bakken shale beds and 50% for the middle member (this choice of values was informed by the compilation of porosity reduction curves for different lithologies in Giles, 1997; North, 1985) and 2) that the pore-fluid was initially similar in composition to modern seawater. An adjustment was made based on the considerations of Machel and Anderson (1989, pg. 907) to account for the amount of Mg^{2+} that would remain dissolved in solution under equilibrium conditions of calcite dolomitization (at 50°C / 122°F, every 1 cm^3 of expelled fluid would contain 3.64×10^{-5} moles of Mg^{2+} *available* for dolomitization, which amounts to only ~2/3 of the concentration in seawater of 5.52×10^{-5} moles/cm^3). *Accordingly, the first major outcome of the mass-balance analysis is that the compaction water volume expelled from each of the three Bakken members – if not enriched in dissolved Mg^{2+} above the concentration level of modern seawater – could have only provided a small portion (~0.5 Gt) of the Mg required to account for the modal dolomite content of the middle Bakken member (23 Gt Mg required) and the under- and overlying shale beds (4 and 5 Gt Mg required, respectively; see Table 3).*

The total amount of dissolved Mg^{2+} potentially released into the pore-fluid throughout the course of clay mineral diagenesis was estimated for each of the three Bakken members as follows. Rock mass was first converted to the mass of illite (rock mass *x* average clay mass fraction *x* 0.93, the average mass fraction of illite in the clay mineral assemblage of the Bakken Fm. as a whole). It should be noted that included under the heading of "mass of illite" is the mixed-layer I/S fraction of the present-day clay mineral assemblage. X-ray diffraction analyses indicate a low percentage (10-30%) of what are presumably *remaining* expandable (smectitic) layers, suggesting that the mixed-layer I/S fraction could be regarded as a mineralogically evolved residual of the smectite illitization process (mixed-layer I/S comprises approx. one-half of the illite+I/S+smectite content, which in-turn comprises, on average, 93% of the entire clay mass in the Bakken Fm.). The mass of illite was then converted to the equivalent mass of smectite by assuming an average smectite composition with a molar mass of 402.7 g/cm^3 (calculated here using examples of structural formulas given by Chamley, 1989, which contain, on average, 1.49 mols Mg^{2+} per mol smectite). Based on the above discussion regarding choice of a reasonable initial smectite-richness value, the resulting quantity was lastly multiplied by 0.65 to arrive at the estimated mass of initial smectite at the time of deposition, from which the size of the clay mineral-hosted Mg-reservoir was finally estimated for each of the three Bakken members (Table 3). *This leads to the second major outcome of the mass-balance analysis. Mainly, for the Bakken Fm. as a whole, the estimated size of the Mg-reservoir (36 Gt) presumably once-hosted by the clay mineral assemblage is sufficient to account for the amount of Mg sequestered during dolomitization (32 Gt).*

In more detail, both the upper and lower Bakken shales are dolomite-poor but clay-rich compared to the middle Bakken reservoir interval (Figs. 2 and 4d). We attribute the low dolomite abundance of the shale beds to a generally low abundance of precursor calcium-carbonate. The results of the mass-balance analysis suggest that the cumulative Mg-availability in the shale beds exceeded the Mg-demand of dolomitization by a factor of ~2.5-3 (Table 3), leaving a substantial excess for potential export and migration through – along with expelled fluids – more transmissive adjacent strata. For example, the up-dip movement of Mg-charged compaction and clay-dehydration waters originating from the lower shale, along with a supplementary flux of fluid from the upper shale, could be considered a viable mechanism for balancing the supply and demand of

Mg for dolomitizing the middle Bakken facies package (where the internal Mg-reservoirs would have been sufficient to account for only ~50% of the Mg now sequestered by dolomite; Table 3). Mass-balance may also be achievable for the middle member by further study of its Stage I dolomite and the associated Mg-requirement. A downward adjustment may be necessary once it is established what – if any – portion of Stage I dolomite is detrital in origin (as has been speculated in the literature) or precipitated while the sediment remained in diffusive contact with seawater (which would have served as a functionally infinite Mg reservoir under such circumstances; *c.f.*, Sass and Katz, 1982).

7. CONCLUDING REMARKS

Dolomitization of the mixed package of carbonate-clastic facies of the middle Bakken tight-oil reservoir (Late Devonian – Early Mississippian, Williston Basin) apparently unfolded in four stages according to the concentric zonation observed in replacive dolomite crystals with respect to Fe-content and the isotopic composition of carbon and oxygen ($\delta^{13}C$ and $\delta^{18}O$, respectively).

A compilation of data on the mineralogical composition of the middle Bakken member in cores from across the Williston Basin shows no major difference in the abundance of dolomite in shallow (~0.5 to 1 km / 1,650 to 3,250 ft) *vs.* deep (~3.5 km / 11,500 ft) burial settings. Within the context of a recent re-evaluation of the burial and thermal history of the Bakken Fm. (Kuhn et al. 2012), pervasive dolomitization of the middle Bakken reservoir (dolomite Stages I and II) is thus restricted to temperatures <70°C (160°F) and depths <1.5 km (5,000 ft), and is restricted in time to the first ~30 m.y. following deposition in the general vicinity of the Williston Basin depocenter. The resulting establishment of a space-supporting framework during the early stages of the burial history contributed significantly to the preservation of porosity and permeability (*c.f.* Weyl, 1960), which are generally both highest where dolomitization of the calcareous fraction of the rock matrix is most severe (calcareous components initially comprised approximately one-half of the bulk sediment mass). The amount of calcareous sediment and clay admixed with silt- and/or fine-sand sized clastic detritus at the time of deposition exerted a major control over how much dolomite would eventually form within each facies during burial. More generally, the abundance and spatial distribution of dolomite – and hence of the favorable reservoir properties that it helps in-part to ensure – follows the abundance and distribution of clays within the silt- and/or fine-sand bearing facies of the middle Bakken member (Facies B-F). This conclusion may be more broadly relevant to designing exploration strategies for similar unconventional tight-oil reservoirs elsewhere.

Based on the outcomes of the Mg mass-balance analysis (Table 3), it is plausible that the Bakken Fm. acquired – along with its clay mineral assemblage at the time of deposition – the latent potential to auto-dolomitize with progressive burial, heating and dewatering. The observed covariance between the clay and dolomite content of middle Bakken facies (Fig. 4b-d) supports the idea that the mass of dissolved Mg^{2+} required to pervasively dolomitize the calcareous fraction of the reservoir rock matrix was sourced in large-part locally from clay-mineral reactions unfolding on a parallel diagenetic track (Fig. 12). Such an internal Mg-source is favorable from the widely-held viewpoint that diagenesis of the middle reservoir member proceeded under closed-system conditions (ensured by the sealing properties of the surrounding shale beds) with respect to extra-formational fluid movements associated with the infilling and burial history of the Williston Basin.

A last gasp of the dolomitization process occurred after late-stage clay dehydration reactions apparently supplied a fresh source of dissolved Mg^{2+} and Fe^{2+} to facilitate the precipitation of a minor volume of ankeritic overgrowths (Stages III and IV), which are best-

developed in vugs and fractures (although smaller equivalents also occupy post-compaction pore-space). Based on fluid inclusion microthermometry, overgrowth precipitation in the general vicinity of the depocenter (Well A, Fig. 1) began at burial depths of ~2.5-3 km (8,200 to 9,850 ft) and temperatures of 116-125°C (241-257°F) and may have continued until the time of maximum burial and heating during the Early Paleogene (~49.5 Ma), when the temperature peaked at 130-140°C (265-285°F; Figs. 1 and 8). For reference, the onset of hydrocarbon generation in Bakken source rocks is thought to have begun at ~110°C (230°F), with maximum generation and expulsion occurring at the time of deepest burial (at ~49.5 Ma, when the temperature in the Bakken depocenter peaked at 165°C / 330°F; Kuhn et al., 2012).

7. REFERENCES

Ahlbrandt, T. S., R. R. Charpentier, T. R. Klett, J. W. Schmoker, C. J. Schenk, and G. F. Ulmishek, 2005, Global Resource Estimates from Total Petroleum Systems: AAPG, 86, 325 p.

Ahmad, N., 1983, Vertisols, *in* Developments in Soil Science: Elsevier, p. 91–123.

Alexandre, C. S., 2011, Reservoir Characterization and Petrology of the Bakken Formation, Elm Coulee Field, Richland County, MT, Ph.D. Dissertation: Colorado School of Mines, Golden, Colorado, 175 p.

Algeo, T. J., R. A. Berner, J. B. Maynard, and S. E. Scheckler, 1995, Late Devonian oceanic anoxic events and biotic crises:"rooted" in the evolution of vascular land plants: GSA today, v. 5, no. 3, p. 45–66.

Algeo, T. J., and S. E. Scheckler, 2010, Land plant evolution and weathering rate changes in the Devonian: Journal of Earth Science, v. 21, no. 1, p. 75–78.

Algeo, T. J., and S. E. Scheckler, 1998, Terrestrial-marine teleconnections in the Devonian: links between the evolution of land plants, weathering processes, and marine anoxic events: Philosophical Transactions of the Royal Society B: Biological Sciences, v. 353, no. 1365, p. 113–130.

Algeo, T. J., S. E. Scheckler, and J. B. Maynard, 2001, Effects of the Middle to Late Devonian Spread of Vascular Land Plants on Weathering Regimes, Marine Biotas, and Global Climate, *in* P. G. Gensel, and D. Edwards, eds., Plants Invade the Land: New York Chichester, West Sussex, Columbia University Press, doi:10.7312/gens11160-013.

Allen, B. L., and D. S. Fanning, 1983, Composition and soil genesis: Developments in Soil Science, v. 11, p. 141–192.

Allison, C. E., R. J. Francey, and H. A. J. Meijer, 1995, Recommendations for the reporting of stable isotope measurements of carbon and oxygen in CO_2 gas, *in* Reference and Intercomparison Materials for Stable Isotopes of Light Elements, Vienna, Austria: International Atomic Energy Agency, p. 155–162.

Almanza, A., 2011, Integrated three dimensional geological model of the Devonian Bakken formation elm coulee field, Williston basin: Richland county Montana, Ph.D. Dissertation: Colorado School of Mines, Golden, Colorado, 140 p.

778 Baertschi, P., 1976, Absolute ^{18}O content of standard mean ocean water: Earth and Planetary Science
779 Letters, v. 31, no. 3, p. 341–344, doi:10.1016/0012-821X(76)90115-1.

780 Barnes, M. A., W. C. Barnes, and R. M. Bustin, 1999, Chemistry and diagenesis of organic matter in
781 sediments: Diagenesis, Geoscience Canada, Reprint Series, v. 4, p. 189–204.

782 Boles, J. R., and S. G. Franks, 1979, Clay diagenesis in Wilcox sandstones of southwest Texas: implications
783 of smectite diagenesis on sandstone cementation: Journal of Sedimentary Research, v. 49, no. 1.

784 Borchardt, G., 1989, Smectites, *in* J. B. Dixon, and S. B. Weed, eds., Minerals in soil environments:
785 Madison, WI, Soil Science Society of America, Inc., p. 675–718.

786 Bottinga, Y., 1968, Calculation of fractionation factors for carbon and oxygen isotopic exchange in the
787 system calcite-carbon dioxide-water: The Journal of Physical Chemistry, v. 72, no. 3, p. 800–808.

788 Brennan, S. W., 2016, Integrated characterization of Middle Bakken diagenesis, Williston Basin, North
789 Dakota, USA, Master's thesis: Colorado School of Mines, Golden, Colorado, 155 p.

790 Brodie, M., 2016, Diagenesis & Reservoir Quality of the Middle Bakken Formation, Ph.D. Dissertation:
791 Durham University, Durham, United Kingdom, 306 p.

792 Brodie, M. W., A. C. Aplin, B. Hart, I. J. Orland, J. W. Valley, and A. J. Boyce, 2018, Oxygen Isotope
793 Microanalysis By Secondary Ion Mass Spectrometry Suggests Continuous 300-million-year History
794 of Calcite Cementation and Dolomitization in the Devonian Bakken Formation: Journal of
795 Sedimentary Research, v. 88, no. 1, p. 91–104.

796 Brown, P. E., and S. Hagemann, 1994, MacFlinCor: a computer program for fluid inclusion data reduction
797 and manipulation, *in* B. DeVivo, and M. L. Frezzotti, eds., Fluid inclusions in minerals: Methods
798 and applications: Blacksburg, Virginia, Virginia Polytechnic Institute and State University Press, p.
799 231–250.

800 Burst, J. F., 1969, Diagenesis of Gulf Coast clayey sediments and its possible relation to petroleum
801 migration: AAPG bulletin, v. 53, no. 1, p. 73–93.

802 Carpenter, A. B., 1980, The chemistry of dolomite formation I: The stability of dolomite: SEPM (Society for
803 Sedimentary Geology), p. 111–121, doi:10.2110/pec.80.28.0111.

804 Carpenter, S. J., and K. C. Lohmann, 1989, $\delta^{18}O$ and $\delta^{13}C$ variations in Late Devonian marine cements from
805 the Golden Spike and Nevis reefs, Alberta, Canada: Journal of Sedimentary Research, v. 59, no. 5,
806 p. 792–814, doi:10.1306/212F9075-2B24-11D7-8648000102C1865D.

807 Chamley, H., 1989, Clay Sedimentology: Berlin Heidelberg, Springer-Verlag.

808 Christopher, J. E., 1961, Transitional Devonian-Mississippian formations of southern Saskatchewan,
809 Geological Report 66: Government of Saskatchewan, 103 p.

810 Coplen, T. B., C. Kendall, and J. Hopple, 1983, Comparison of stable isotope reference samples: Nature, v.
811 302, no. 5905, p. 236–238, doi:10.1038/302236a0.

812 Craig, H., 1957, Isotopic standards for carbon and oxygen and correction factors for mass-spectrometric
813 analysis of carbon dioxide: Geochimica et cosmochimica acta, v. 12, no. 1, p. 133–149.

814 Domeier, M., and T. H. Torsvik, 2014, Plate tectonics in the late Paleozoic: Geoscience Frontiers, v. 5, no.
815 3, p. 303–350, doi:10.1016/j.gsf.2014.01.002.

816 Edwards, W. W., 1993, Sedimentology and diagenesis of the Bakken Formation in Daly Field, southwest
817 Manitoba, Master's thesis: University of Manitoba, Winnipeg, Manitoba, 201 p.

818 Egenhoff, S., A. V. Dolah, A. Jaffri, and J. Maletz, 2011, Facies Architecture and Sequence Stratigraphy of
819 the Middle Bakken Member, North Dakota, *in* J. W. Robinson, J. A. LeFever, and S. B. Gaswirth,
820 eds., The Bakken-Three Forks Petroleum System in the Williston Basin: Rocky Mountain
821 Association of Geologists, Denver, Colorado, p. 27–47.

822 Ferdous, H., 2001, Regional Sedimentology and Diagenesis of the Middle Bakkan Member: Implications
823 for Reservoir Rock Distribution in Southern Saskatchewan, Ph.D. Dissertation: University of
824 Saskatchewan, Saskatoon, Saskatchewan, 467 p.

825 Foscolos, A. E., I. A. McIlreath, and D. W. Morrow, 1990, Catagenesis of argillaceous sedimentary rocks:
826 Diagenesis: Geosciences Canadian Reprint Series IV, p. 177–188.

827 Friedman, I., and J. R. O'Neil, 1977, Compilation of stable isotope fractionation factors of geochemical
828 interest, *in* Data of Geochemistry Sixth Edition: United States Government Printing Office,
829 Washington, Geological Survey Professional Paper 440-KK, p. 116.

830 Galloway, W. E., 1984, Hydrogeologic regimes of sandstone diagenesis: Clastic diagenesis: AAPG Memoir,
831 v. 37, p. 3–13.

832 Gaswirth, S. B. et al., 2013, Assessment of undiscovered oil resources in the bakken and three forks
833 formations, Williston Basin Province, Montana, North Dakota, and South Dakota, 2013: US
834 Geological Survey Fact Sheet, v. 3013, no. 4.

835 Gaswirth, S. B., and K. R. Marra, 2015, U.S. Geological Survey 2013 assessment of undiscovered resources
836 in the Bakken and Three Forks Formations of the U.S. Williston Basin Province: AAPG Bulletin, v.
837 99, no. 04, p. 639–660, doi:10.1306/08131414051.

838 van Geldern, R., M. M. Joachimski, J. Day, U. Jansen, F. Alvarez, E. A. Yolkin, and X.-P. Ma, 2006, Carbon,
839 oxygen and strontium isotope records of Devonian brachiopod shell calcite: Palaeogeography,
840 Palaeoclimatology, Palaeoecology, v. 240, no. 1–2, p. 47–67, doi:10.1016/j.palaeo.2006.03.045.

841 Gerhard, L. C., S. B. Anderson, J. A. Lefever, and C. G. Carlson, 1982, Geological development, origin, and
842 energy mineral resources of Williston Basin, North Dakota: AAPG Bulletin, v. 66, no. 8, p. 989–
843 1020.

844 Ghosh, P., J. Adkins, H. Affek, B. Balta, W. Guo, E. A. Schauble, D. Schrag, and J. M. Eiler, 2006, 13C–18O
845 bonds in carbonate minerals: A new kind of paleothermometer: Geochimica et Cosmochimica
846 Acta, v. 70, no. 6, p. 1439–1456, doi:10.1016/j.gca.2005.11.014.

847 Giles, M. R., 1997, Diagenesis: A quantitative perspective: Dordrecht, Kluwer Academic, 526 p.

Goldstein, R. H., 2001, Fluid inclusions in sedimentary and diagenetic systems: Lithos, v. 55, no. 1, p. 159–193, doi:10.1016/S0024-4937(00)00044-X.

Goldstein, R. H., and T. J. Reynolds (eds.), 1994, Systematics of Fluid Inclusions in Diagenetic Minerals: SEPM (Society for Sedimentary Geology), doi:10.2110/scn.94.31.

Goldstein, R. H., I. Samson, and A. Anderson, 2003, Petrographic analysis of fluid inclusions: Fluid inclusions: Analysis and interpretation, v. 32, p. 9–53.

Gosnold, W. D., 1990, Heat flow in the Great Plains of the United States: Journal of Geophysical Research: Solid Earth, v. 95, no. B1, p. 353–374.

Gregg, J. M., D. L. Bish, S. E. Kaczmarek, and H. G. Machel, 2015, Mineralogy, nucleation and growth of dolomite in the laboratory and sedimentary environment: A review: Sedimentology, v. 62, no. 6, p. 1749–1769, doi:10.1111/sed.12202.

Grover, P. W., 1996, Stratigraphy and diagenesis of the Mississippian Bakken shale-Lodgepole Limestone sequence, Williston basin, North Dakota, Ph.D. Dissertation: Texas A & M University, College Station, 207 p.

Hauck, T. E., D. Pană, and S. A. DuFrane, 2017, Northern Laurentian provenance for Famennian clastics of the Jasper Basin (Alberta, Canada): A Sm-Nd and U-Pb detrital zircon study: Geosphere, p. GES01453.1, doi:10.1130/GES01453.1.

Hesse, R., 1999, Early diagenetic pore water/sediment interaction: Diagenesis, Geoscience Canada, Reprint Series, v. 4, p. 277–316.

Horita, J., 2014, Oxygen and carbon isotope fractionation in the system dolomite–water–CO2 to elevated temperatures: Geochimica et Cosmochimica Acta, v. 129, p. 111–124, doi:10.1016/j.gca.2013.12.027.

Hower, J., E. V. Eslinger, M. E. Hower, and E. A. Perry, 1976, Mechanism of burial metamorphism of argillaceous sediment: 1. Mineralogical and chemical evidence: Geological Society of America Bulletin, v. 87, no. 5, p. 725, doi:10.1130/0016-7606(1976)87<725:MOBMOA>2.0.CO;2.

Hurley, N. F., and K. C. Lohmann, 1989, Diagenesis of Devonian reefal carbonates in the Oscar Range, Canning Basin, Western Australia: Journal of Sedimentary Research, v. 59, no. 1, p. 127–146, doi:10.1306/212F8F35-2B24-11D7-8648000102C1865D.

Ibrahim, T. I., 2014, Provenance of Early Mississippian Bakken clastics based on detrital zircon and detrital conodonts, Abstract: GSA Annual Meeting in Vancouver, British Columbia, 19-22 October.

Irwin, H., C. Curtis, and M. Coleman, 1977, Isotopic evidence for source of diagenetic carbonates formed during burial of organic-rich sediments: Nature, v. 269, p. 209–213.

Kaiser, S. I., M. Aretz, and R. T. Becker, 2016, The global Hangenberg Crisis (Devonian–Carboniferous transition): review of a first-order mass extinction: Geological Society, London, Special Publications, v. 423, no. 1, p. 387–437, doi:10.1144/SP423.9.

Kaiser, S. I., T. Steuber, R. T. Becker, and M. M. Joachimski, 2006, Geochemical evidence for major environmental change at the Devonian–Carboniferous boundary in the Carnic Alps and the Rhenish Massif: Palaeogeography, Palaeoclimatology, Palaeoecology, v. 240, no. 1–2, p. 146–160, doi:10.1016/j.palaeo.2006.03.048.

Karasinski, D. R., 2006, Sedimentology and hydrocarbon potential of the Devonian Three Forks and Mississippian Bakken Formations, Sinclair Area, southeast Saskatchewan-southwest Manitoba, Master's thesis: University of Manitoba, Winnipeg, Manitoba, 436 p.

Kent, D. M., and J. E. Christopher, 1994, Geological history of the Williston Basin and Sweetgrass arch: Geological Atlas of the Western Canada Sedimentary Basin, p. 421–430.

Kohlruss, D., and E. Nickel, 2013, Bakken Formation of southeastern Saskatchewan–selected stratigraphy and production maps: Saskatchewan Ministry of the Economy, Saskatchewan Geological Survey, Open File, v. 1.

LeFever, J. A., 1992, Horizontal Drilling in the Williston Basin, United States and Canada, *in* J. W. Schmoker, E. B. Coalson, and C. A. Brown, eds., Geological studies relevant to horizontal drilling: Examples from Western North America: Rocky Mountain Association of Geologists, Denver, Colorado, p. 177–198.

LeFever, J. A., 2008, Isopach of the Bakken Formation (5 sheets): North Dakota Geological Survey, North Dakota Geological Survey, Geologic Investigations No. 59.

Lefever, J. A., C. D. Martiniuk, E. F. R. Dancsok, and P. A. Mahnic, 1991, Petroleum potential of the middle member, Bakken Formation, Williston Basin, *in* Sixth International Williston Basin Symposium: p. 74–94.

Listiono, G. A., 2016, Mixed siliciclastic-carbonate system of the middle member of the Bakken Formation, Williston Basin, North Dakota, Master's thesis: Colorado School of Mines, Golden, Colorado, 168 p.

Longinelli, A., and S. Nuti, 1973, Revised phosphate-water isotopic temperature scale: Earth and Planetary Science Letters, v. 19, no. 3, p. 373–376, doi:10.1016/0012-821X(73)90088-5.

Lucia, F. J., 1995, Rock-Fabric/Petrophysical Classification of Carbonate Pore Space for Reservoir Characterization: AAPG Bulletin, v. 79, no. 9, p. 1275–1300.

Luz, B., Y. Kolodny, and J. Kovach, 1984, Oxygen isotope variations in phosphate of biogenic apatites, III. Conodonts: Earth and Planetary Science Letters, v. 69, no. 2, p. 255–262, doi:10.1016/0012-821X(84)90185-7.

Machel, H. G., 2004, Concepts and models of dolomitization: a critical reappraisal: Geological Society, London, Special Publications, v. 235, no. 1, p. 7–63, doi:10.1144/GSL.SP.2004.235.01.02.

Machel, H. G., 1997, Recrystallization versus neomorphism, and the concept of 'significant recrystallization'in dolomite research: Sedimentary Geology, v. 113, no. 3, p. 161–168.

Machel, H. G., 1987, Saddle dolomite as a by-product of chemical compaction and thermochemical sulfate reduction: Geology, v. 15, no. 10, p. 936–940.

Machel, H. G., and J. H. Anderson, 1989, Pervasive subsurface dolomitization of the Nisku Formation in central Alberta: Journal of Sedimentary Research, v. 59, no. 6, p. 891–911, doi:10.1306/212F90AC-2B24-11D7-8648000102C1865D.

Machel, H. G., and E. W. Mountjoy, 1986, Chemistry and environments of dolomitization—a reappraisal: Earth-Science Reviews, v. 23, no. 3, p. 175–222.

Machel, H. G., and E. W. Mountjoy, 1987, General constraints on extensive pervasive dolomitization–and their application to the Devonian carbonates of western Canada: Bulletin of Canadian Petroleum Geology, v. 35, no. 2, p. 143–158.

Meissner, F. F., 1978, Petroleum geology of the Bakken Formation Williston Basin, North Dakota and Montana, *in* D. Rehig, ed., 1978 Williston Basin Symposium, Billings, Montana: p. 207–227.

Millán, M. I., H. Machel, and S. M. Bernasconi, 2016, Constraining Temperatures of Formation and Composition of Dolomitizing Fluids In the Upper Devonian Nisku Formation (Alberta, Canada) With Clumped Isotopes: Journal of Sedimentary Research, v. 86, no. 2, p. 107–112, doi:10.2110/jsr.2016.6.

Milliken, K. L., 2003, Late Diagenesis and Mass Transfer in Sandstone Shale Sequences, *in* F. T. Mackenzie, ed., Treatise on Geochemistry Volume 7: Sediments, Diagenesis, and Sedimentary Rocks (2nd Edition): Elsevier, p. 446.

Mora, C. I., S. G. Driese, and P. G. Seager, 1991, Carbon dioxide in the Paleozoic atmosphere: Evidence from carbon-isotope compositions of pedogenic carbonate: Geology, v. 19, no. 10, p. 1017–1020, doi:10.1130/0091-7613(1991)019<1017:CDITPA>2.3.CO;2.

Nandy, D., 2017, Dolomitization and porosity evolution of Middle Bakken member, Elm Coulee field and facies characterization, chemostratigraphy and organic-richness of Upper Bakken shale, Williston Basin, Ph.D. Dissertation: Colorado School of Mines, Golden, Colorado, 212 p.

Nordeng, S. H., J. A. LeFever, F. J. Anderson, M. Bingle-Davis, and E. H. Johnson, 2010, An examination of the factors that impact oil production from the middle member of the Bakken Formation in Mountrail County, North Dakota, Report of Investigation No. 109: North Dakota Geological Survey, North Dakota Department of Mineral Resources, 93 p.

North, F. K., 1985, Petroleum Geology: Boston, Allen & Unwin Inc., 607 p.

Perry, E., and J. Hower, 1970, Burial diagenesis in Gulf Coast pelitic sediments: Clays and Clay Minerals, v. 18, no. 3, p. 165–177.

Perry, E. A., and J. Hower, 1972, Late-stage dehydration in deeply buried pelitic sediments: AAPG Bulletin, v. 56, no. 10, p. 2013–2021.

Peterhänsel, A., B. R. Pratt, and C. Holmden, 2008, The Famennian (Upper Devonian) Palliser Platform of western Canada—architecture and depositional dynamics of a post-extinction epeiric giant: Dynamics of Epeiric Seas: Geological Society of Canada Special Paper, v. 48, p. 247–281.

Peterman, Z., and J. Thamke, 2016, Chemical and isotopic changes in Williston Basin brines during long-term oil production: An example from the Poplar dome, Montana: AAPG Bulletin, v. 100, no. 10, p. 1619–1632, doi:10.1306/05261615114.

Pitman, J. K., L. C. Price, and J. A. LeFever, 2001, Diagenesis and fracture development in the Bakken Formation, Williston Basin: Implications for reservoir quality in the middle member: U.S. Geological Survey Professional Paper 1653, p. 24.

Powers, M. C., 1967, Fluid-release mechanisms in compacting marine mudrocks and their importance in oil exploration: AAPG bulletin, v. 51, no. 7, p. 1240–1254.

Retallack, G. J., 1986, The fossil record of soils, *in* P. V. Wright, ed., Paleosols: their recognition and interpretation: Oxford, Blackwells, p. 1–57.

Rolfs, S., 2015, Integrated Geomechanical, Geophysical, and Geochemical Analysis of the Bakken Formation, Elm Coulee Field, Williston Basin, Montana, Master's thesis: Colorado School of Mines, Golden, Colorado, 138 p.

Rostron, B. J., and C. Holmden, 2000, Fingerprinting formation-waters using stable isotopes, Midale area, Williston Basin, Canada: Journal of Geochemical Exploration, v. 69, p. 219–223.

Sarg, J. F., 2012, The Bakken – An Unconventional Petroleum and Reservoir System: United States Department of Energy National Energy Technology Laboratory, Oil & Natural Gas Technology, 65 p.

Sass, E., and A. Katz, 1982, The origin of platform dolomites; new evidence: American Journal of Science, v. 282, no. 8, p. 1184–1213.

Schneider, C. A., W. S. Rasband, K. W. Eliceiri, and others, 2012, NIH Image to ImageJ: 25 years of image analysis: Nat methods, v. 9, no. 7, p. 671–675.

Scottese, C. R., and W. S. McKerrow, 1990, Revised world maps and introduction: Paleozoic Paleogeography and Biogeography, Geological Society Memoir No, v. 12, p. 1–21.

Shields, M. J., and P. V. Brady, 1995, Mass balance and fluid flow constraints on regional-scale dolomitization, Late Devonian, Western Canada Sedimentary Basin: Bulletin of Canadian Petroleum Geology, v. 43, no. 4, p. 371–392.

Sibley, D. F., and J. M. Gregg, 1987, Classification of dolomite rock textures: Journal of Sedimentary Research, v. 57, no. 6, p. 967–975.

Skoreyko, D., 2017, Hydrogeological Characterization of the Bakken Aquifer, Williston Basin (Canada-USA), Master's thesis: University of Alberta, University of Alberta, 171 p.

Śliwiński, M. G., K. Kitajima, R. Kozdon, M. J. Spicuzza, A. Denny, and J. W. Valley, 2017, In situ $\delta^{13}C$ and $\delta^{18}O$ microanalysis by SIMS: A method for characterizing the carbonate components of natural and engineered CO2-reservoirs: International Journal of Greenhouse Gas Control, v. 57, p. 116–133, doi:10.1016/j.ijggc.2016.12.013.

Śliwiński, M. G., K. Kitajima, R. Kozdon, M. J. Spicuzza, J. H. Fournelle, A. Denny, and J. W. Valley, 2016a, Secondary Ion Mass Spectrometry Bias on Isotope Ratios in Dolomite–Ankerite, Part I: $\delta^{18}O$ Matrix Effects: Geostandards and Geoanalytical Research, v. 40, no. 2, p. 157–172, doi:10.1111/j.1751-908X.2015.00364.x.

Śliwiński, M. G., K. Kitajima, R. Kozdon, M. J. Spicuzza, J. H. Fournelle, A. Denny, and J. W. Valley, 2016b, Secondary Ion Mass Spectrometry Bias on Isotope Ratios in Dolomite–Ankerite, Part II: $\delta^{13}C$ Matrix Effects: Geostandards and Geoanalytical Research, v. 40, no. 2, p. 173–184, doi:10.1111/j.1751-908X.2015.00380.x.

Smith, M. G., 1996, The Bakken Formation (Late Devonian-Early Mississippian): A black shale source rock in the Williston basin, Ph.D. Dissertation: University of British Columbia, 807 p.

Smith, M. G., and R. M. Bustin, 1998, Production and preservation of organic matter during deposition of the Bakken Formation (Late Devonian and Early Mississippian), Williston Basin: Palaeogeography, Palaeoclimatology, Palaeoecology, v. 142, no. 3, p. 185–200.

Sonnenberg, S. A., J. A. LeFever, and R. J. Hill, 2011, Fracturing in the Bakken petroleum system, Williston Basin, *in* J. W. Robinson, J.A. LeFever, and S. B. Gaswirth, eds., The Bakken-Three Forks Petroleum System in the Williston Basin: Rocky Mountain Association of Geologists, p. 393–417.

Sonnenberg, S. A., and A. Pramudito, 2009, Petroleum geology of the giant Elm Coulee field, Williston Basin: AAPG Bulletin, v. 93, no. 9, p. 1127–1153, doi:10.1306/05280909006.

Sorensen, J., D. . Schmidt, and S. A. Smith, 2010, Subtask 1.2-Evaluation of Key Factors Affecting Successful Oil Production in the Bakken Formation, North Dakota, DE-FC26-08NT43291: United States Department of Energy National Energy Technology Laboratory, 106 p.

Staruiala, A. B., 2016, Sedimentology, Diagenesis (Including Dolomitization) of the Bakken Formation, Southeastern Saskatchewan, Canada, Master's thesis: University of Regina, Regina, Saskatchewan, 402 p.

Stoakes, F. A., 1980, Nature and Control of Shale Basin Fill and its Effect on Reef Growth and Termination: Upper Devonian Duvernay and Ireton Formations of Alberta, Canada: Bulletin of Canadian Petroleum Geology, v. 28, no. 3, p. 345–410.

Streel, M., M. V. Caputo, S. Loboziak, and J. H. G. Melo, 2000, Late Frasnian–Famennian climates based on palynomorph analyses and the question of the Late Devonian glaciations: Earth-Science Reviews, v. 52, no. 1–3, p. 121–173.

Valley, J. W., and N. T. Kita, 2009, In situ oxygen isotope geochemistry by ion microprobe, *in* M. Fayek, ed., Secondary ion mass spectrometry in the earth sciences: gleaning the big picture from a small spot: Mineralogical Association of Canada (MAC), p. 19–63.

Warren, J., 2000, Dolomite: occurrence, evolution and economically important associations: Earth-Science Reviews, v. 52, no. 1, p. 1–81.

Webster, R. L., 2011, Chapter 19: Petroleum Source Rocks and Stratigraphy of the Bakken Formation in North Dakota: p. 490–507.

Weijermars, R., K. Paradis, E. Belostrino, F. Feng, T. Lal, A. Xie, and C. Villareal, 2017, Re-appraisal of the Bakken Shale play: Accounting for historic and future oil prices and applying fiscal rates of North Dakota, Montana and Saskatchewan: Energy Strategy Reviews, v. 16, p. 68–95, doi:10.1016/j.esr.2017.02.005.

Wendte, J., and T. Uyeno, 2005, Sequence stratigraphy and evolution of Middle to Upper Devonian Beaverhill Lake strata, south-central Alberta: Bulletin of Canadian Petroleum Geology, v. 53, no. 3, p. 250–354.

Wescott, A., 2016, Reservoir characterization of the Middle Bakken Member, Fort Berthold Region, North Dakota, Williston Basin, Master's thesis: Colorado School of Mines, Golden, Colorado, 193 p.

Weyl, P. K., 1960, Porosity through dolomitization: conservation-of-mass requirements: Journal of Sedimentary Research, v. 30, no. 1.

Whalen, M. T., and J. E. Day, 2008, Magnetic susceptibility, biostratigraphy, and sequence stratigraphy: insights into Devonian carbonate platform development and basin infilling, Western Alberta: Society for Sedimentary Geology, v. 89, p. 291–314.

Whitney, G., and H. R. Northrop, 1988, Experimental investigation of the smectite to illite reaction: Dual reaction mechanisms and oxygen-isotope systematics: American Mineralogist, v. 73, p. 77–90.

Wilkinson, M., S. F. Crowley, and J. D. Marshall, 1992, Model for the evolution of oxygen isotope ratios in the pore fluids of mudrocks during burial: Marine and Petroleum Geology, v. 9, no. 1, p. 98–105.

Wilson, M. J., M. V. Shaldybin, and L. Wilson, 2016, Clay mineralogy and unconventional hydrocarbon shale reservoirs in the USA. I. Occurrence and interpretation of mixed-layer R3 ordered illite/smectite: Earth-Science Reviews, v. 158, p. 31–50, doi:10.1016/j.earscirev.2016.04.004.

Zenger, D. H., J. B. Dunham, and R. L. Ethington (eds.), 1980, Concepts and Models of Dolomitization: SEPM Special Publication, 320 p.

Zhang, Y.-G., and J. D. Frantz, 1987, Determination of the homogenization temperatures and densities of supercritical fluids in the system NaClKClCaCl2H2O using synthetic fluid inclusions: Chemical Geology, v. 64, no. 3–4, p. 335–350.

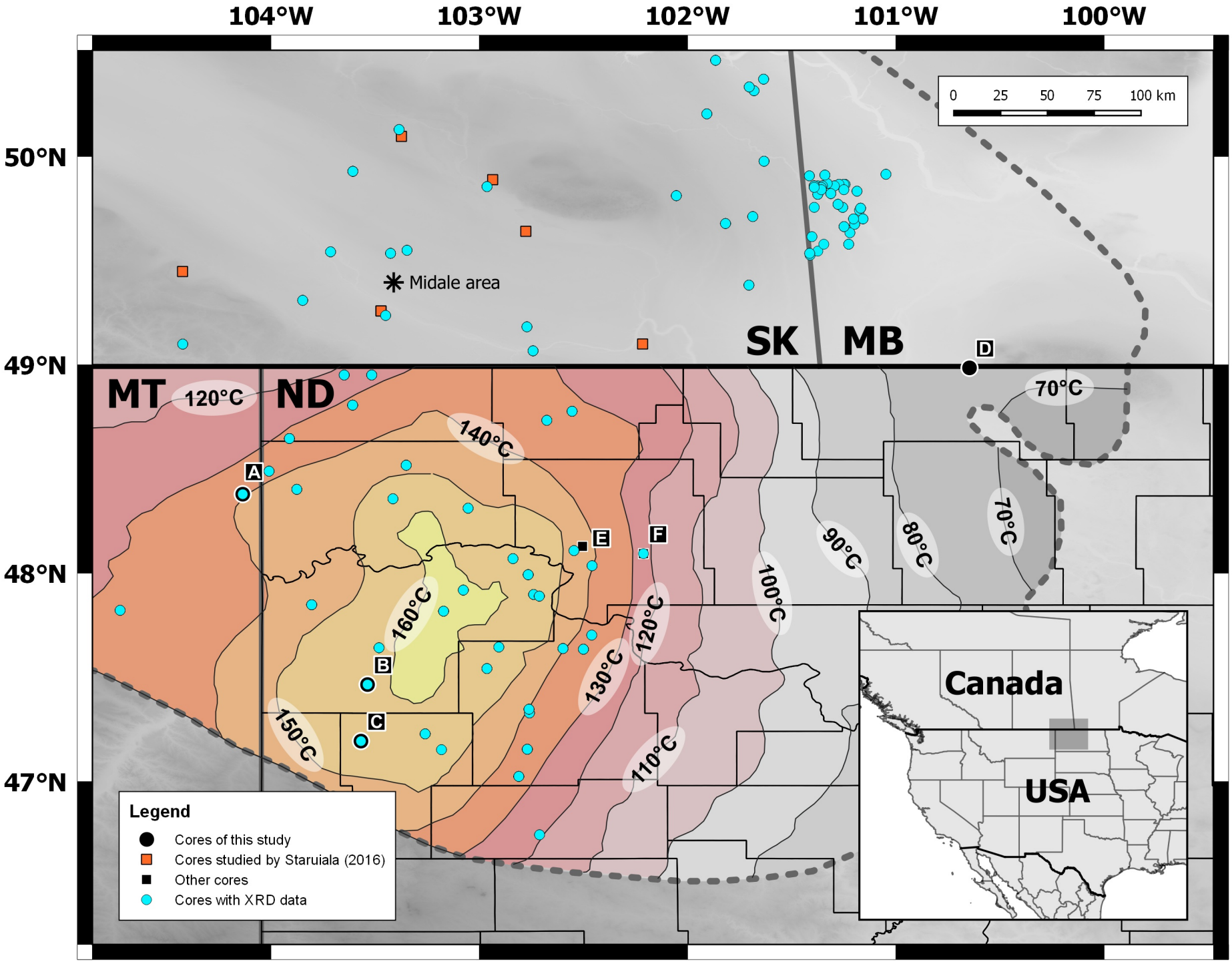
104°W
103°W
102°W
101°W
100°W
50°N
49°N
48°N
47°N
0 25 50 75 100 km
Midale area
SK
MB
MT
ND
120°C
140°C
160°C
150°C
130°C
120°C
110°C
100°C
90°C
80°C
70°C
70°C
A
B
C
D
E
F
Canada
USA
Legend
Cores of this study
Cores studied by Staruiala (2016)
Other cores
Cores with XRD data

Figure 2

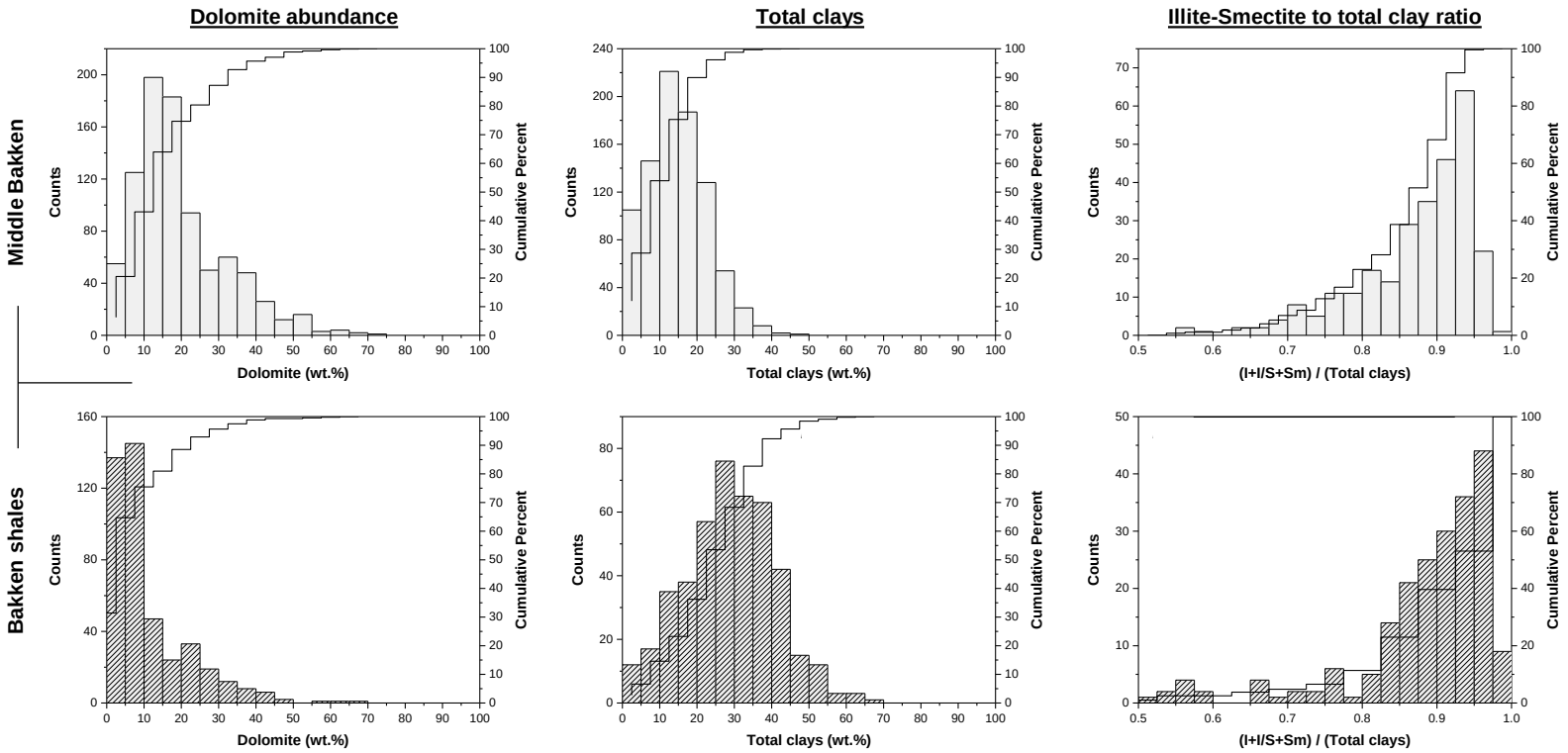
Dolomite abundance
Total clays
Illite-Smectite to total clay ratio
Middle Bakken
Bakken shales
Counts
Cumulative Percent
Dolomite (wt.%)
Total clays (wt.%)
(I+I/S+Sm) / (Total clays)

Figure 3

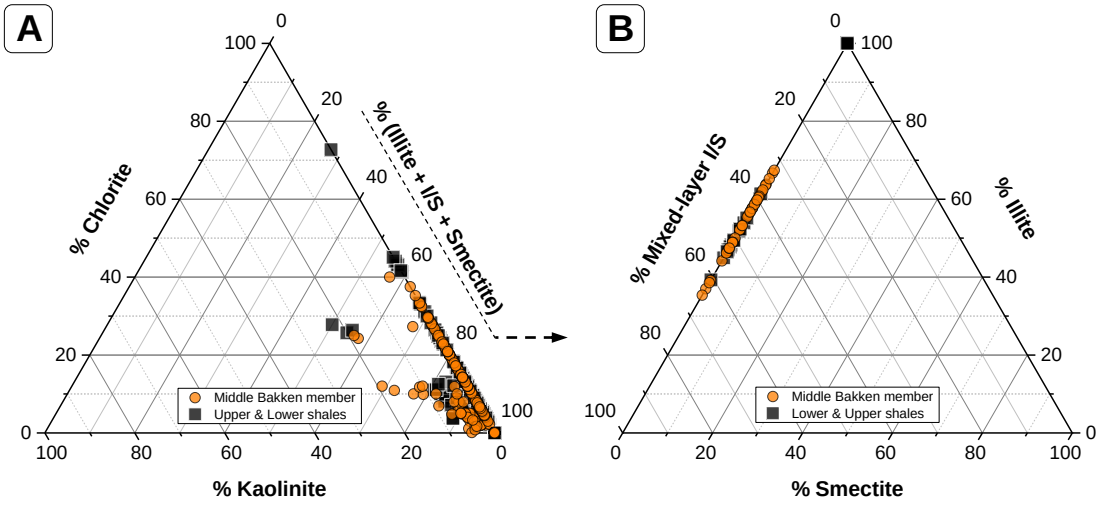
A
% Chlorite
% (Illite + IIS + Smectite)
% Kaolinite
Middle Bakken member
Upper & Lower shales
B
% Mixed-layer IIS
% Illite
% Smectite
Middle Bakken member
Lower & Upper shales

Figure 4

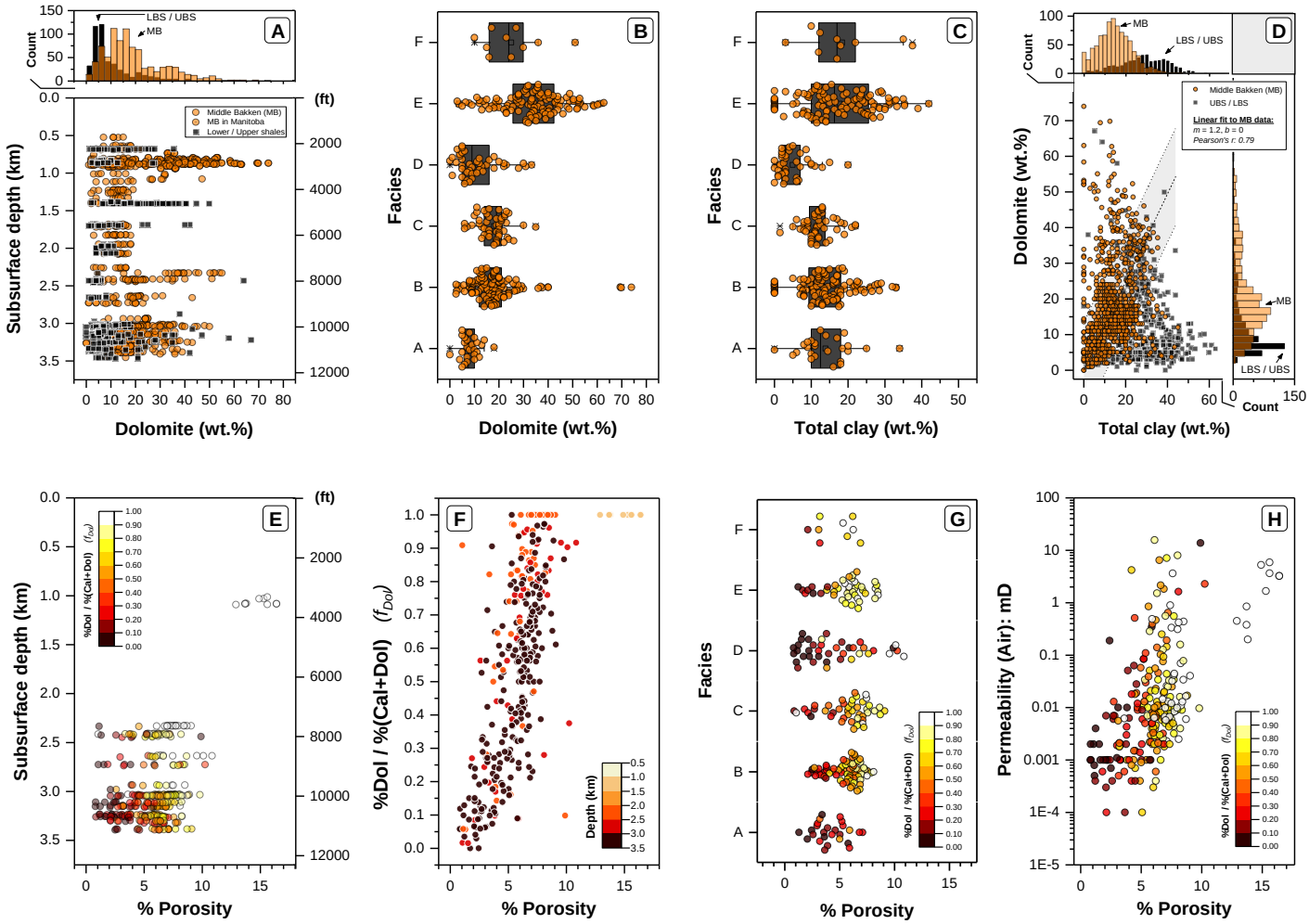
A
LBS / UBS
MB
Count
Middle Bakken (MB)
MB in Manitoba
Lower / Upper shales
Subsurface depth (km)
(ft)
Dolomite (wt.%)
B
Facies
C
Total clay (wt.%)
D
Linear fit to MB data:
m = 1.2, b = 0
Pearson's r: 0.79
Dolomite (wt.%)
E
%Dol / %(Cal+Dol) (fDol)
% Porosity
F
Depth (km)
G
H
Permeability (Air): mD

Figure 5

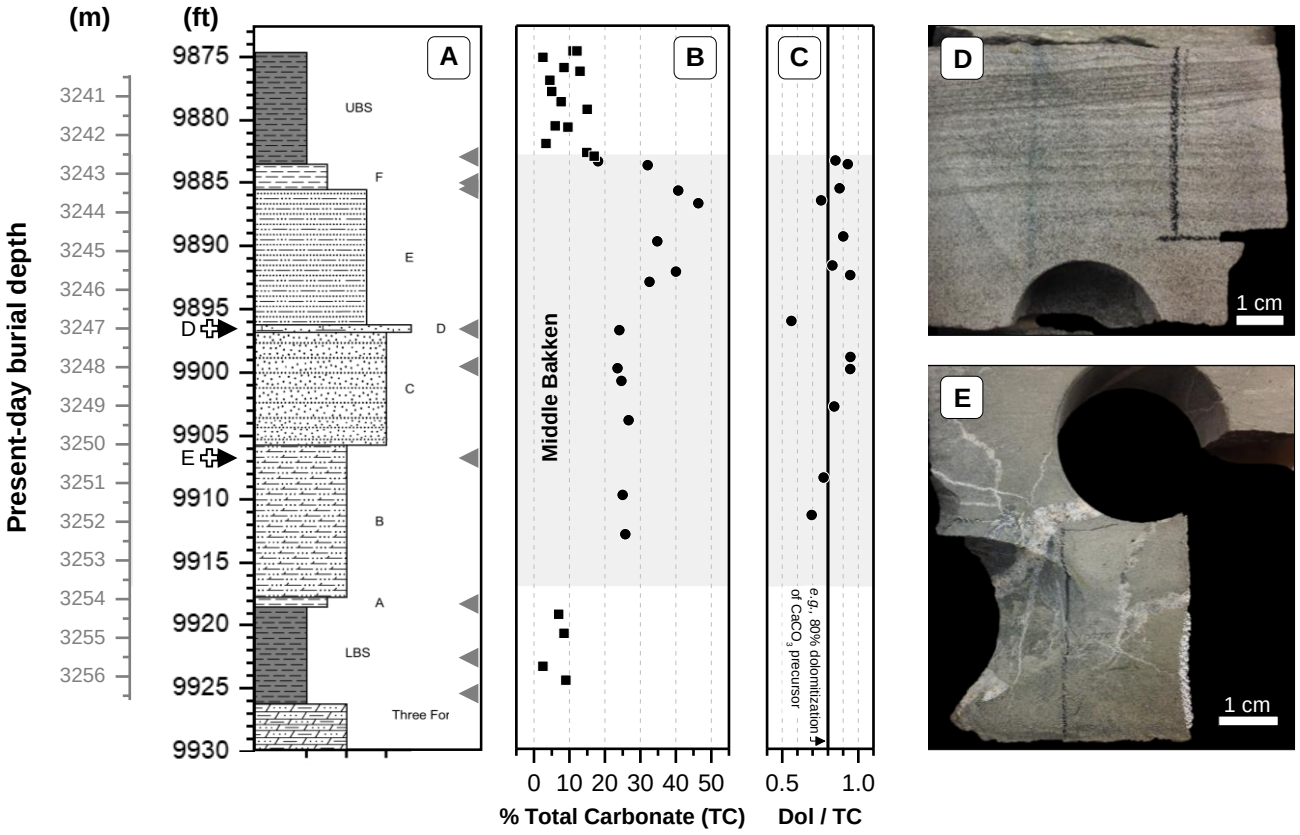
(m)
(ft)
Present-day burial depth
3241
3242
3243
3244
3245
3246
3247
3248
3249
3250
3251
3252
3253
3254
3255
3256
9875
9880
9885
9890
9895
9900
9905
9910
9915
9920
9925
9930
A
UBS
F
E
D
C
B
A
LBS
Three For
D
E
B
Middle Bakken
0 10 20 30 40 50
% Total Carbonate (TC)
0.5 1.0
DoI / TC
e.g., 80% dolomitization of CaCO3 precursor
D
1 cm
E
1 cm

Figure 6

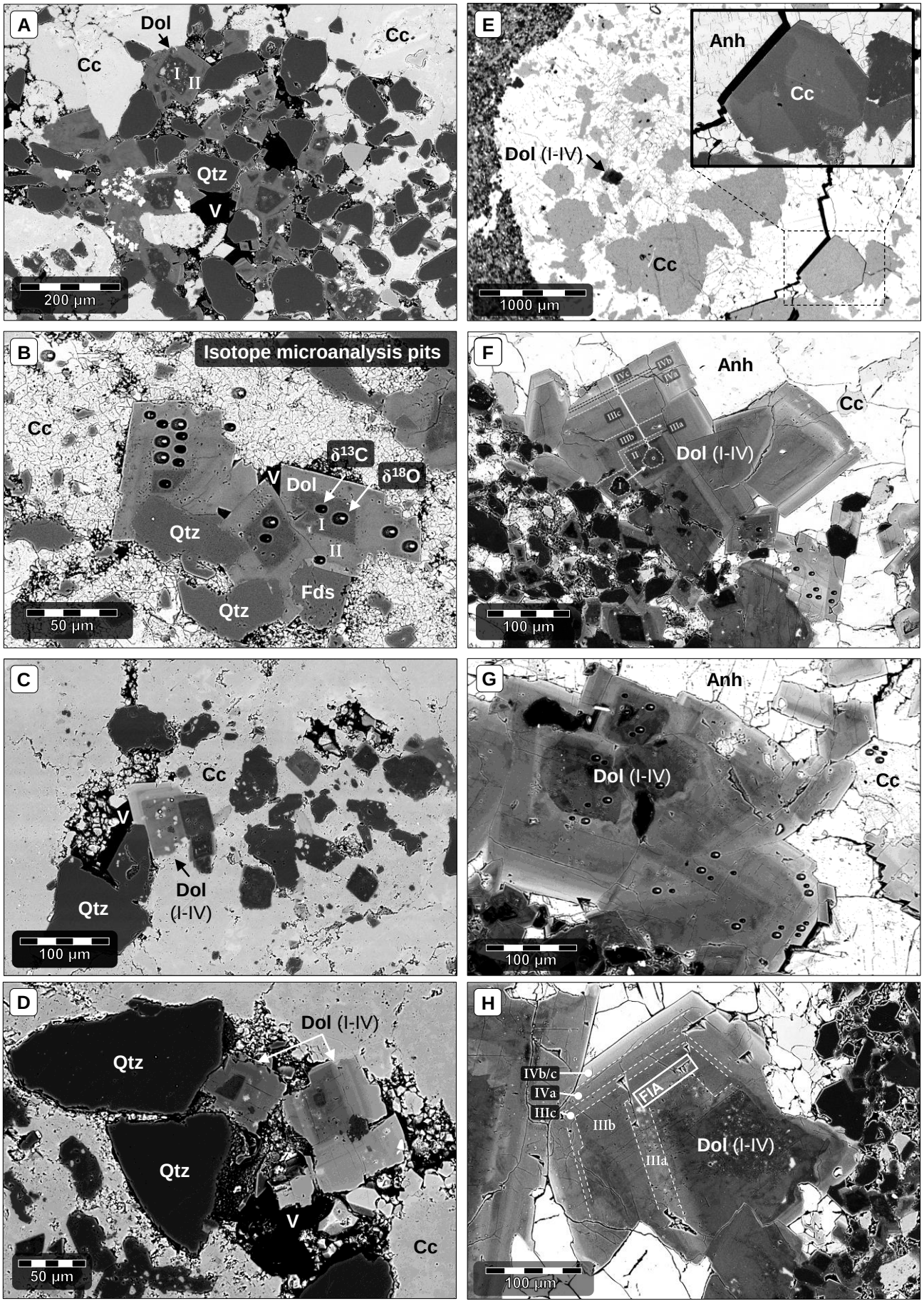
A
Dol
Cc
Cc
I
II
Qtz
V
200 µm
B
Isotope microanalysis pits
Cc
δ13C
δ18O
V
Dol
I
II
Qtz
Fds
Qtz
50 µm
C
Cc
V
Dol
(I-IV)
Qtz
100 µm
D
Dol (I-IV)
Qtz
Qtz
V
Cc
50 µm
E
Anh
Cc
Dol (I-IV)
Cc
1000 µm
F
Anh
IVc
IVb
IVa
Cc
IIIc
IIIa
IIIb
II
Dol (I-IV)
I
100 µm
G
Anh
Dol (I-IV)
Cc
100 µm
H
IVb/c
IVa
IIIc
FIA
IIIb
IIIa
Dol (I-IV)
100 µm

Figure 7

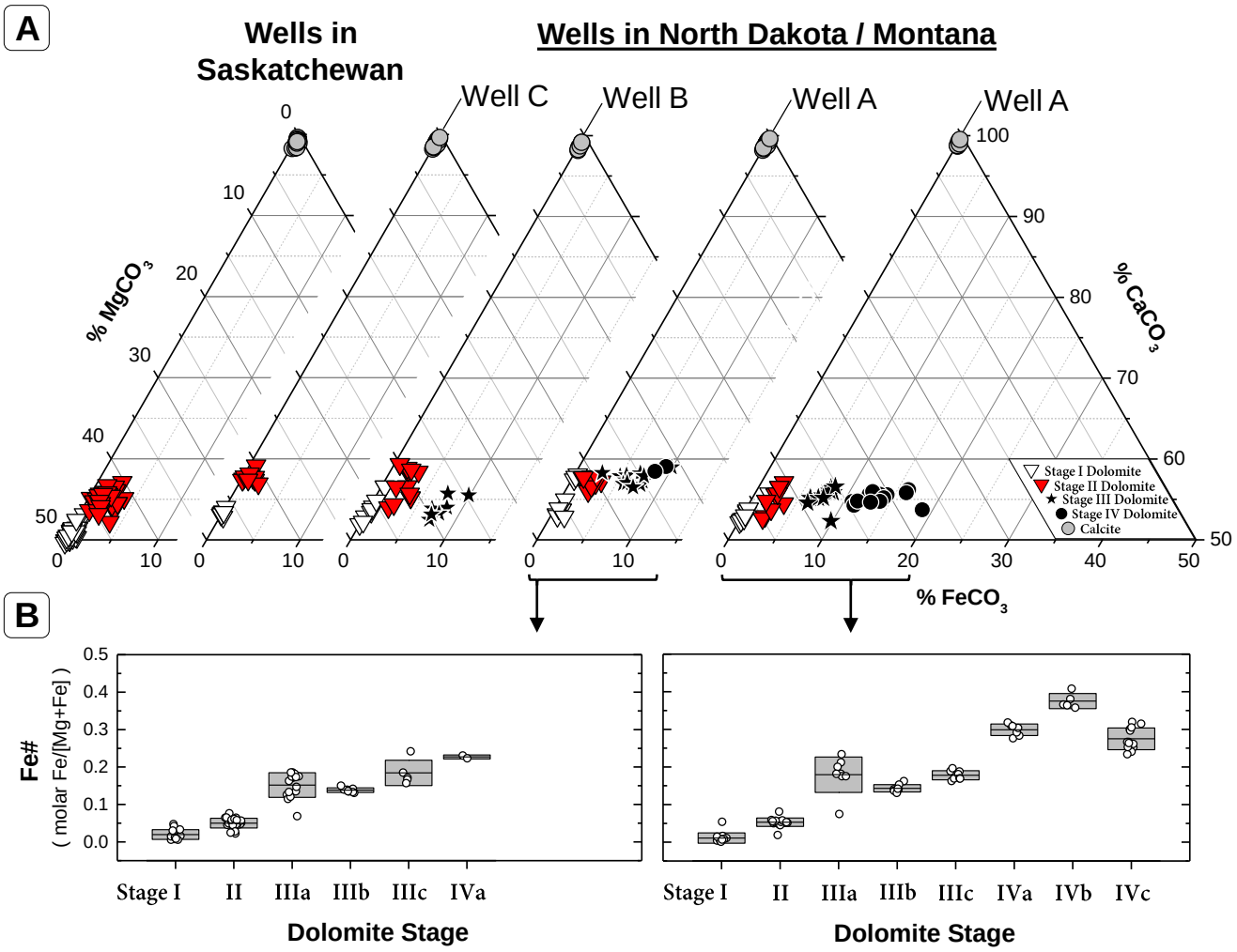
A
Wells in Saskatchewan
Wells in North Dakota / Montana
Well C
Well B
Well A
Well A
% MgCO3
% CaCO3
% FeCO3
Stage I Dolomite
Stage II Dolomite
Stage III Dolomite
Stage IV Dolomite
Calcite
B
Fe#
(molar Fe/[Mg+Fe])
Stage I
II
IIIa
IIIb
IIIc
IVa
IVb
IVc
Dolomite Stage

Figure 8

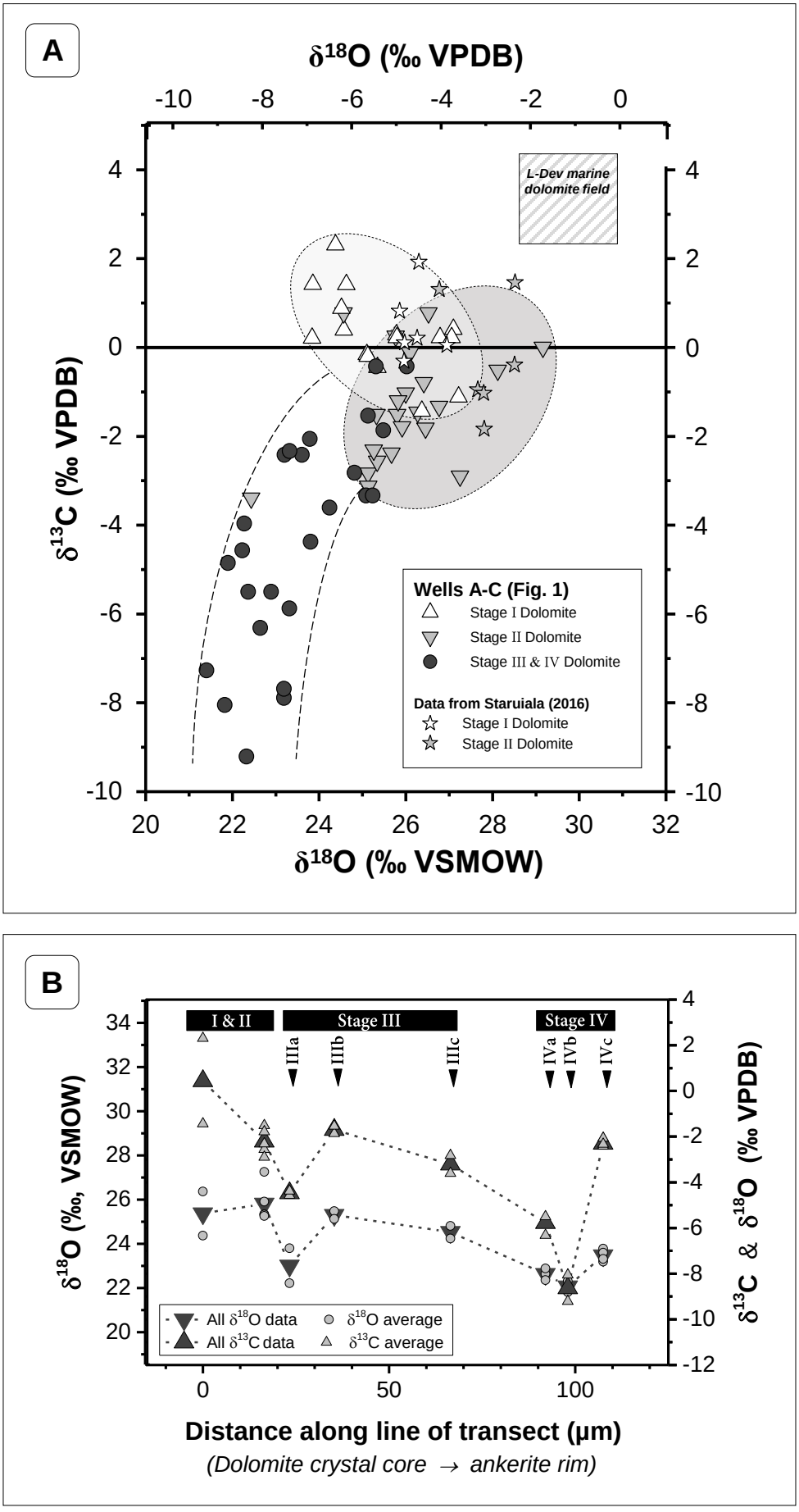
A
δ18O (‰ VPDB)
δ13C (‰ VPDB)
δ18O (‰ VSMOW)
L-Dev marine dolomite field
Wells A-C (Fig. 1)
Stage I Dolomite
Stage II Dolomite
Stage III & IV Dolomite
Data from Staruiala (2016)
Stage I Dolomite
Stage II Dolomite
B
I & II
Stage III
Stage IV
IIIa
IIIb
IIIc
IVa
IVb
IVc
δ18O (‰, VSMOW)
δ13C & δ18O (‰ VPDB)
All δ18O data
δ18O average
All δ13C data
δ13C average
Distance along line of transect (μm)
(Dolomite crystal core → ankerite rim)

Figure 9

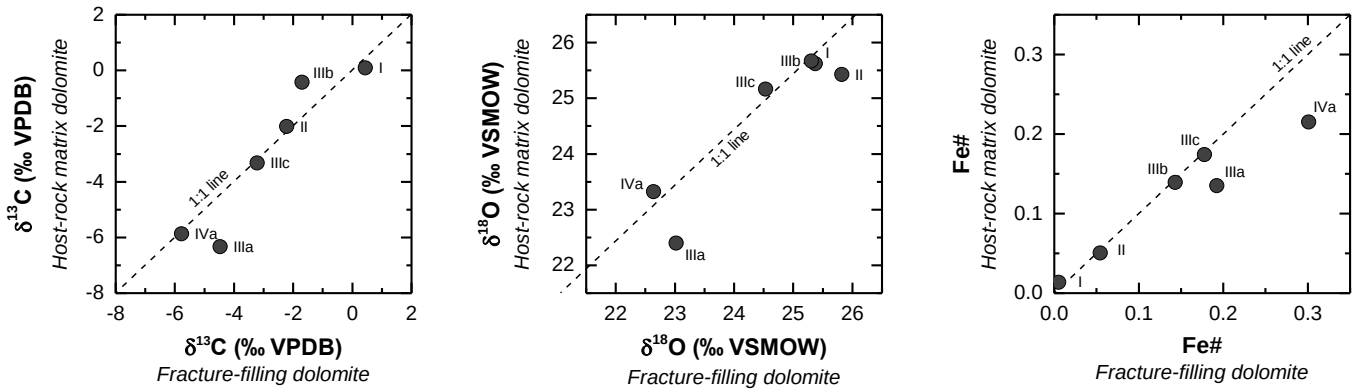
δ13C (‰ VPDB)
Host-rock matrix dolomite
δ13C (‰ VPDB)
Fracture-filling dolomite
1:1 line
I
II
IIIa
IIIb
IIIc
IVa
δ18O (‰ VSMOW)
Host-rock matrix dolomite
δ18O (‰ VSMOW)
Fracture-filling dolomite
Fe#
Host-rock matrix dolomite
Fe#
Fracture-filling dolomite

Figure 10

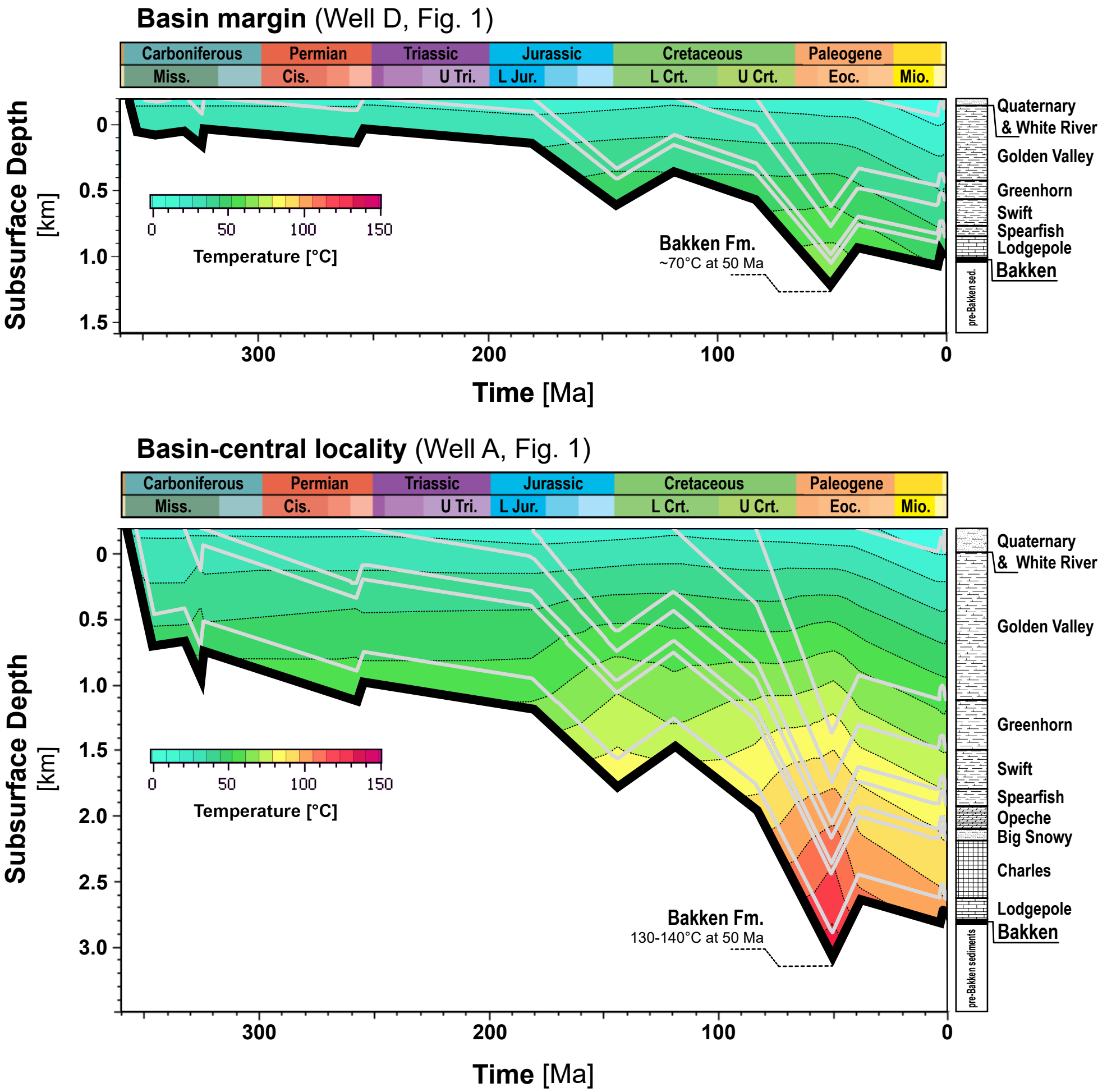
Basin margin (Well D, Fig. 1)
Carboniferous
Permian
Triassic
Jurassic
Cretaceous
Paleogene
Miss.
Cis.
U Tri.
L Jur.
L Crt.
U Crt.
Eoc.
Mio.
Subsurface Depth [km]
0
0.5
1.0
1.5
0
50
100
150
Temperature [°C]
Bakken Fm.
~70°C at 50 Ma
300
200
100
0
Time [Ma]
Quaternary & White River
Golden Valley
Greenhorn
Swift
Spearfish
Lodgepole
Bakken
pre-Bakken sed.
Basin-central locality (Well A, Fig. 1)
Carboniferous
Permian
Triassic
Jurassic
Cretaceous
Paleogene
Miss.
Cis.
U Tri.
L Jur.
L Crt.
U Crt.
Eoc.
Mio.
Subsurface Depth [km]
0
0.5
1.0
1.5
2.0
2.5
3.0
0
50
100
150
Temperature [°C]
Bakken Fm.
130-140°C at 50 Ma
300
200
100
0
Time [Ma]
Quaternary & White River
Golden Valley
Greenhorn
Swift
Spearfish
Opeche
Big Snowy
Charles
Lodgepole
Bakken
pre-Bakken sediments

Figure 11

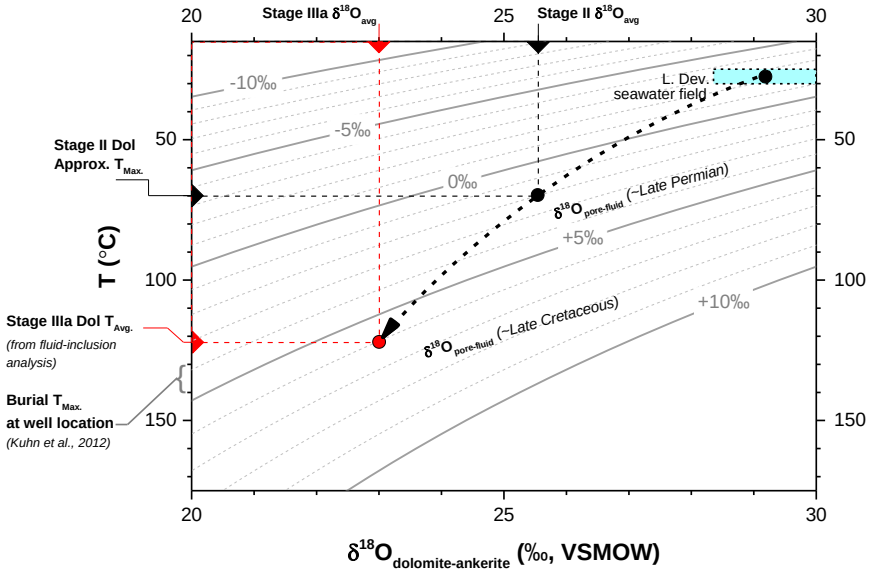
Stage IIIa δ18Oavg
Stage II δ18Oavg
20
25
30
-10‰
-5‰
0‰
+5‰
+10‰
L. Dev. seawater field
δ18Opore-fluid (~Late Permian)
δ18Opore-fluid (~Late Cretaceous)
Stage II Dol Approx. TMax.
Stage IIIa Dol TAvg. (from fluid-inclusion analysis)
Burial TMax. at well location (Kuhn et al., 2012)
T (°C)
50
100
150
δ18Odolomite-ankerite (‰, VSMOW)

Figure 12

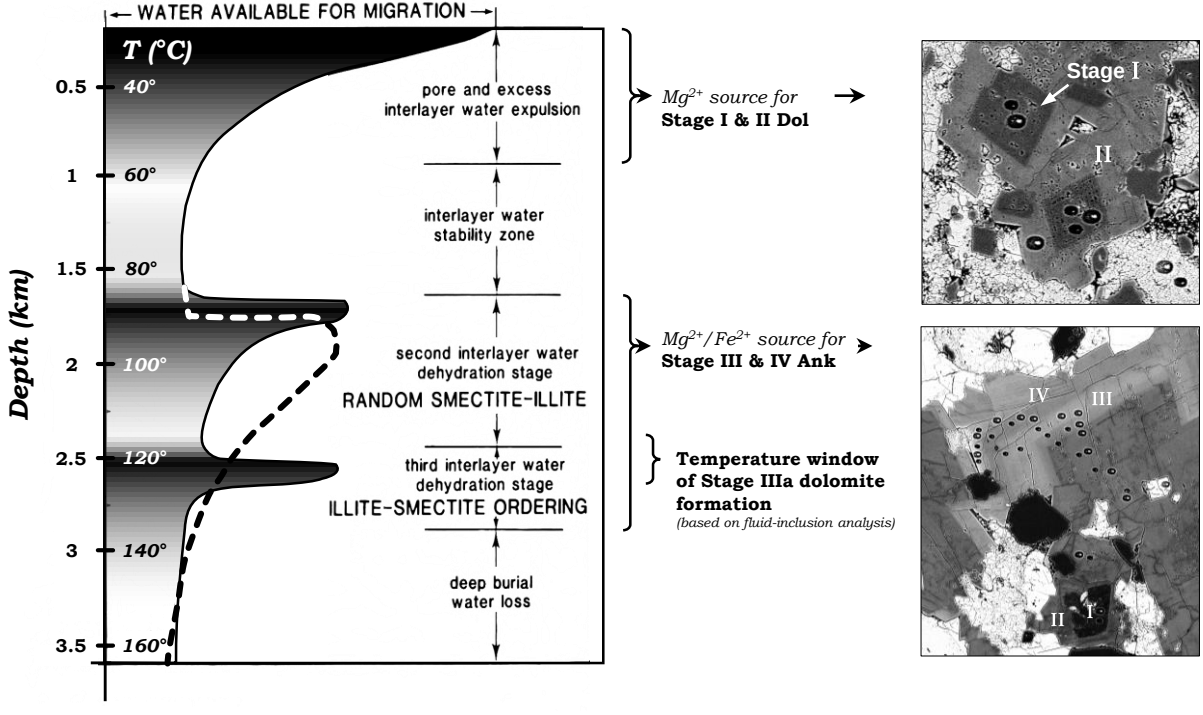
WATER AVAILABLE FOR MIGRATION
T (°C)
Depth (km)
0.5
40°
1
60°
1.5
80°
2
100°
2.5
120°
3
140°
3.5
160°
pore and excess interlayer water expulsion
interlayer water stability zone
second interlayer water dehydration stage
RANDOM SMECTITE-ILLITE
third interlayer water dehydration stage
ILLITE-SMECTITE ORDERING
deep burial water loss
Mg2+ source for
Stage I & II Dol
Mg2+/Fe2+ source for
Stage III & IV Ank
Temperature window of Stage IIIa dolomite formation
(based on fluid-inclusion analysis)
Stage I
II
IV
III
II
I

FIGURE AND TABLE CAPTIONS

Fig. 1. Map of study area. Approximate limit of Bakken Fm. shown by dashed line. Thermal contours indicate maximum alteration temperatures at time of maximum burial (after Fig. 6a of Kuhn et al., 2012). Core identifiers: A = E701, B = B832, C = D284 (A-C held by USGS CRC), D = 24883 (held by NDGS), E = Deadwood Canyon Ranch 43-28H, F = Wayzetta 46-11M (E & F: refer to Brennan, 2016).

Fig. 2. (A) Major clay groups and their relative abundances in the clay fraction of the Bakken Fm. **(B)** Relative abundances of smectite, mixed-layer I/S and illite in the clay fraction of the Bakken Fm.

Fig. 3. Clay-mineral and dolomite abundance distributions in the Bakken Fm. *(Top row)* Middle Bakken member. *(Bottom row)* Lower and Upper Bakken shales. Note that illite-smectite group clays dominate the clay fraction. At present, the illite-smectite group is a mixture of sub-equal parts illite (I) and mixed-layer illite/smectite (I/S) which contains only a small percentage (~10-30%) of expandable (*i.e.,* smectitic) layers. The low expandability can be interpreted as a residual of the temperature-driven process of smectite-illitization that commonly takes place in marine sediments during the first several kilometers of burial (*e.g.,* Chamley, 1989).

Fig. 4. Plots showing the distribution of dolomite in middle Bakken reservoir facies and its relation to clay content, porosity and permeability. Localities represented by the dataset are shown in Figure 1 (denoted as “cores with XRD data (middle Bakken)). **(A)** Dolomite *vs.*

present-day burial depth; **(B)** Dolomite distribution shown on a facies-specific basis; **(C)** Clay distribution shown on a facies-specific basis; **(D)** Total clay *vs.* dolomite content; **(E)** Porosity *vs.* present-day burial depth. Data points color-coded according to the extent of dolomitization of the carbonate fraction (wt.% dolomite / wt.%(calcite + dolomite); **(F)** Porosity *vs*. fractional dolomitization. Data points color-coded according to present-day depth; **(G)** Porosity values plotted on a facies-specific basis. Data points color-coded according to fractional dolomitization; **(H)** Porosity *vs.* permeability (air). Data points color-coded according to fractional dolomitization.

Fig. 5. **Stratigraphy of the middle Bakken member (A) and distribution of total carbonate (calcite + dolomite) (B) in Well A** (see Fig. 1). Shown in **(C)** is the extent of dolomitization of the carbonate fraction ("fractional dolomitization" as in Fig. 2). Crossed-arrows labeled "D" and "F" indicate recovery depth of samples shown in panels **(D)** and **(F)**.

Fig. 6. Petrographic images of multi-generational dolomite in the middle Bakken reservoir. In these backscattered-electron images, compositional zonation (concentric banding) shows up as different shades of gray: darkest tones correspond to non-ferroan dolomite (crystal cores), whereas progressively lighter tones indicate an increase in Fe-content. Examples of Dolomite Stages I and II in **(A)** a shallow burial setting (Well D in Fig. 1; 1.1 km/3,743.4 ft) and **(B)** a deep burial setting (Well B; 3.3 km/10,967 ft). **(C and D)** Dolomite Stages I-IV in Well #16586 (NDGS), situated in the general vicinity of Wells E and F in Fig. 1 (depth: 3.0 km/9,812 ft). Note that Stages III and IV fill post-compaction pore-space. Refer to panel **(F)**, which shows a labeled example of the full zoning sequence. **(E-H)** The coarsest and most extensively zoned dolomite

crystals are encountered lining the walls of fractures and vugs (Well A, 3.0 km/9906.9 ft). Cc = Calcite; Dol = Dolomite; Qtz = Quartz; Fds = Feldspar; Anh = Anhydrite; V = Void space.

Fig. 7. Plots showing the compositional evolution of dolomite in the middle Bakken reservoir (determined by EPMA). Shown also is the range of encountered calcite compositions. **(A)** Carbonate ternary diagrams (Ca-Mg-Fe). Well locations shown in Figure 1. Data for wells in Saskatchewan from Staruiala (2016). **(B)** Amount of Fe^{2+} substituting for Mg^{2+} at each stage of dolomite crystal growth (Fe# = Fe/(Mg+Fe), expressed on a molar basis). Plot to left shows data for sample shown in panel D of Fig. 3 (dolomite in host-rock matrix; Well A, 3.0 km/9896.6 ft). Plot to right shows data for sample shown in panel E of Fig. 3 (fracture-filling dolomite; Well A, 3.0 km/9906.9 ft).

Fig. 8. Plots showing the evolution of stable carbon and oxygen isotope ratios in multi-generational dolomite of the middle Bakken reservoir. (A) Cross-plot of $\delta^{13}C$ and $\delta^{18}O$ values. Hatched field indicates range of hypothetical dolomite compositions in equilibrium with Late Devonian seawater at 25-30°C (see text for discussion). Data for dolomite Stages I and II provides cross-basin coverage. Data for Stages III and IV is specific to Well A. **(B)** Composite transect showing core-to-rim evolution of dolomite $\delta^{13}C$ and $\delta^{18}O$ (scaled to line of transect shown in Fig. 4(F).

Fig. 9. A zone-by-zone comparison of dolomite chemistry in extension fractures *vs.* host-rock matrix. The near 1:1 correspondence of measured Fe-concentrations *(inset)* and isotopic

signatures ($\delta^{13}C$ and $\delta^{18}O$ – *main plot*) points to a common diagenetic history. The coarsest examples of Stage 3 & 4 dolomite are encountered in vugs and fractures, where they preserve the most extensive record of pore-fluid $\delta^{18}O$ evolution during burial. The same zoning sequence can be encountered in the low-porosity and low-permeability host rock, although the very latest sub-zones are frequently either absent or too thin to accommodate a 6-μm diameter $\delta^{13}C$ analysis spot

Fig. 10. Burial and thermal history (360 Ma to present) of the Bakken Fm. at two different localities in the US Williston Basin: (A) a shallow burial setting on the basin margin in north-central North Dakota (Well D in Fig. 1; present-day burial depth of 1.1 km), and **(B)** a deep burial setting in a more basin-central locality in northeastern Montana (Well A in Fig. 1; present-day burial depth of 3.0 km). The reconstruction for the basin margin restricts the formation of dolomite Stages I and II (the bulk of the dolomite volume in middle Bakken reservoir facies; see Fig. 4) to the first kilometer of burial and/or temperatures not exceeding ~70°C. Both reconstructions were extracted from the PetroMod model of Kuhn et al. (2012).

Fig. 11. Plot showing evolution of pore-fluid $\delta^{18}O$ during dolomitization. Lines of constant water composition calculated using the temperature-dependent relation of Horita (2014) for oxygen isotope partitioning between dolomite and water during precipitation at equilibrium conditions.

Fig. 12. Standard water escape curves for shaley sediments rich in smectitic (swelling) clays at deposition and the inferred relation to pulses of dolomitization of middle Bakken

reservoir facies. Filled solid curve after Perry and Hower (1972), dashed curve after Burst (1969). Redrawn from Fig. 15.14 of Chamley (1989). Depth-scale adjusted to reflect the average paleogeothermal gradient of 40°C/km in the Williston Basin (after Gosnold, 1990; Pitman et al., 2001).

Table 1. Isotopic composition ($\delta^{13}C$ and $\delta^{18}O$ by SIMS) and major element chemistry (by EPMA) of multi-generational dolomite in the middle Bakken reservoir.

Table 2. Results of fluid inclusion analysis in calcite and dolomite of the middle Bakken reservoir (Well A, Sample A; refer to Fig. 1).

Table 3: By the numbers: The Mg demands of dolomitization *vs.* the estimated size of internal Mg-reservoirs (clays and compaction waters) for the Bakken Fm. of North Dakota.

Supplementary Appendix 1. SIMS and EPMA datasets.

Supplementary Appendix 2. Petrographic documentation of all sample regions analyzed by SIMS (*in situ*, micron-scale $\delta^{18}O$ and $\delta^{13}C$ analyses), with individually annotated analysis pits.

Supplementary Appendix 3. Supporting petrographic documentation for analyzed fluid inclusion assemblages in calcite and dolomite of the middle Bakken member (Well A, refer to Fig. 1).

Table 1.

Analysis ID ($\delta^{18}O$)	$\delta^{18}O$ (‰) (VSMOW)	$\delta^{18}O$ (‰) (VPDB)	2SD	Fe#	Analysis ID ($\delta^{13}C$)	$\delta^{13}C$ (‰) (VPDB)	2SD	Fe#	Dist. from Core:	Min.	Stage	Note
Well A, Sample A (3.020 km / 9906.9 ft)												
20160817@153.asc	26.4	-4.4	0.2	0.006	20160804@500.asc	-1.4	0.4	0.007	0	NFD	I	Euhedral core
20160817@154.asc	24.4	-6.3	0.2	0.005	20160804@527.asc	2.3	0.6	0.004	0.0	NFD	I	Euhedral core
Avg.	**25.4**	**-5.4**	**0.2**	**0.005**	-	**0.4**	**0.5**	**0.005**	-	-	-	-
20160817@138.asc	25.3	-5.4	0.2	0.055	20160804@493.asc	-2.6	0.4	0.051	16.5	NFD	II	-
20160817@131.asc	25.3	-5.4	0.2	0.051	20160804@522.asc	-1.5	0.6	0.054	16.5	NFD	II	-
20160817@152.asc	27.3	-3.5	0.2	0.037	20160804@524.asc	-2.9	0.6	0.056	16.5	NFD	II	-
20160817@137.asc	25.3	-5.5	0.2	0.058	20160804@492.asc	-2.3	0.4	0.053	16.5	NFD	II	-
20160817@136.asc	25.9	-4.8	0.2	0.049	20160804@523.asc	-1.8	0.6	0.081	16.5	NFD	II	-
Avg.	**25.8**	**-4.9**	**0.2**	**0.050**	-	**-2.2**	**0.5**	**0.059**	-	-	-	-
2SD	**1.7**	**1.6**	**0.0**	**0.016**	-	**1.1**	**0.3**	**0.025**	-	-	-	-
20160817@122.asc	22.2	-8.4	0.2	0.179	20160804@498.asc	-4.6	0.4	0.179	23.3	FD	IIIa	-
20160817@130.asc	23.8	-6.9	0.2	0.206	20160804@521.asc	-4.4	0.6	0.206	23.3	Ank	IIIa	-
20160817@129.asc	25.5	-5.3	0.2	0.137	20160804@496.asc	-1.9	0.4	0.140	35.3	FD	IIIb	-
20160817@123.asc	25.1	-5.6	0.2	0.158	20160804@497.asc	-1.5	0.4	0.139	35.3	FD	IIIb	-
20160817@127.asc	24.2	-6.5	0.2	0.188	20160804@495.asc	-3.6	0.4	0.188	66.5	FD	IIIc	-
20160817@128.asc	24.8	-5.9	0.2	0.169	20160804@499.asc	-2.8	0.4	0.166	66.5	FD	IIIc	-
Avg.	**24.3**	**-6.4**	**0.2**	**0.173**	-	**-3.1**	**0.4**	**0.170**	-	-	-	-
2SD	**2.3**	**2.3**	**0.0**	**0.049**	-	**2.5**	**0.2**	**0.054**	-	-	-	-
20160817@125.asc	22.6	-8.0	0.2	0.283	20160804@519.asc	-6.3	0.6	0.283	92.0	Ank	IVa	-
20160817@124.asc	22.9	-7.8	0.2	0.302	20160804@520.asc	-5.5	0.6	0.313	92.0	Ank	IVa	-
20160817@126.asc	22.4	-8.3	0.2	0.313	20160804@520.asc	-5.5	0.6	0.313	92.0	Ank	IVa	-
20160817@143.asc	21.8	-8.8	0.2	0.408	20160804@509.asc	-8.0	0.4	0.369	98.0	Ank	IVb	-
20160817@142.asc	22.3	-8.3	0.2	0.365	20160804@513.asc	-9.2	0.4	0.369	98.0	Ank	IVb	-
20160817@140.asc	23.8	-6.9	0.2	0.247	20160804@507.asc	-2.1	0.4	0.252	107.5	Ank	IVc	-
20160817@144.asc	23.6	-7.1	0.2	0.306	20160804@511.asc	-2.4	0.4	0.266	107.5	Ank	IVc	-
20160817@145.asc	23.2	-7.5	0.2	0.284	20160804@511.asc	-2.4	0.4	0.266	107.5	Ank	IVc	-
20160817@141.asc	23.3	-7.4	0.2	0.253	20160804@512.asc	-2.3	0.4	0.240	107.5	Ank	IVc	-
Avg.	**22.9**	**-7.8**	**0.2**	**0.307**	-	**-4.9**	**0.5**	**0.297**	-	-	-	-
2SD	**1.3**	**1.3**	**0.0**	**0.103**	-	**5.4**	**0.3**	**0.096**	-	-	-	-
Well A, Sample B (3.016 km / 9896.6 ft)												
20160817@255.asc	23.8	-6.9	0.4	0.032	20160805@586.asc	0.2	0.5	0.021	-	NFD	I	-
20160817@207.asc	26.8	-4.0	0.3	0.017	20160805@602.asc	0.2	0.5	0.012	-	NFD	I	Fossil frag. core
20160817@208.asc	25.8	-5.0	0.3	0.015	20160805@602.asc	0.2	0.5	0.012	-	NFD	I	Fossil frag. core
20160817@215.asc	27.1	-3.7	0.3	0.009	20160805@602.asc	0.2	0.5	0.012	-	NFD	I	Fossil frag. core
20160817@209.asc	25.1	-5.6	0.3	0.012	20160805@603.asc	-0.2	0.5	0.008	-	NFD	I	Fossil frag. core
20160817@210.asc	25.1	-5.6	0.3	0.006	20160805@604.asc	-0.2	0.5	0.006	-	NFD	I	Fossil frag. core
Avg.	**25.6**	**-5.1**	**0.3**	**0.015**	-	**0.1**	**0.5**	**0.012**	-	-	-	-
2SD	**2.4**	**2.3**	**0.1**	**0.018**	-	**0.4**	**0.1**	**0.011**	-	-	-	-
20160817@235.asc	22.4	-8.2	0.4	0.045	20160805@578.asc	-3.4	0.7	0.048	-	NFD	II	-
20160817@236.asc	25.8	-4.9	0.4	0.046	20160805@583.asc	-1.2	0.5	0.050	-	NFD	II	-
20160817@240.asc	26.3	-4.5	0.4	0.026	20160805@585.asc	-1.5	0.5	0.026	-	NFD	II	-
20160817@238.asc	25.1	-5.6	0.4	0.060	20160805@587.asc	-2.8	0.5	0.055	-	NFD	II	-
20160817@237.asc	25.1	-5.6	0.4	0.058	20160805@589.asc	-3.1	0.5	0.050	-	NFD	II	-
20160817@212.asc	26.8	-4.0	0.3	0.060	20160805@606.asc	-1.3	0.5	0.056	-	NFD	II	-
20160817@211.asc	26.4	-4.4	0.3	0.047	20160805@607.asc	-0.8	0.5	0.076	-	NFD	II	-
Avg.	**25.4**	**-5.3**	**0.3**	**0.049**	**-**	**-2.0**	**0.5**	**0.052**	**-**	**-**	**-**	**-**
2SD	**2.9**	**2.8**	**0.1**	**0.024**	**-**	**2.1**	**0.2**	**0.030**	**-**	**-**	**-**	**-**
20160817@230.asc	23.2	-7.5	0.2	0.069	20160805@577.asc	-7.9	0.7	0.131	-	NFD	IIIa	-
20160817@230.asc	23.2	-7.5	0.2	0.069	20160805@584.asc	-7.7	0.5	0.118	-	NFD	IIIa	-
20160817@229.asc	21.9	-8.7	0.2	0.166	20160805@573.asc	-4.9	0.7	0.174	-	FD	IIIa	-
20160817@228.asc	22.3	-8.4	0.2	0.178	20160805@575.asc	-4.0	0.7	0.180	-	FD	IIIa	-
20160817@214.asc	21.4	-9.2	0.3	0.133	20160805@605.asc	-7.3	0.5	0.133	-	FD	IIIa	-
20160817@226.asc	26.0	-4.7	0.2	0.134	20160805@576.asc	-0.4	0.7	0.140	-	FD	IIIb	-
20160817@227.asc	25.3	-5.4	0.2	0.143	20160805@576.asc	-0.4	0.7	0.140	-	FD	IIIb	-
20160817@224.asc	25.1	-5.6	0.2	0.178	20160805@570.asc	-3.3	0.7	0.178	-	FD	IIIc	-
20160817@225.asc	25.2	-5.5	0.2	0.162	20160805@570.asc	-3.3	0.7	0.178	-	FD	IIIc	-

Avg.	**23.7**	**-7.0**	**0.2**	**0.137**	**-**	**-4.4**	**0.7**	**0.152**	**-**	**-**	**-**	**-**
2SD	**3.4**	**3.3**	**0.1**	**0.084**	**-**	**5.7**	**0.2**	**0.050**	**-**	**-**	**-**	**-**
20160817@223.asc	23.3	-7.4	0.2	0.203	20160805@569.asc	-5.9	0.7	0.227	-	Ank	IVa	-

Well B (3.158 km / 10,361 ft)

20160817@333.asc	23.9	-6.8	0.2	0.007	20160807@926.asc	1.4	0.4	0.000	-	NFD	I	Euhedral core
20160817@344.asc	27.1	-3.7	0.2	0.007	20160807@927.asc	0.4	0.4	0.000	-	NFD	I	Euhedral core
20160817@343.asc	27.2	-3.6	0.2	0.008	20160807@933.asc	-1.1	0.4	0.008	-	NFD	I	Euhedral core
20160817@336.asc	24.6	-6.1	0.2	0.005	20160807@934.asc	0.4	0.4	0.011	-	NFD	I	Euhedral core
Avg.	**25.7**	**-5.1**	**0.2**	**0.007**	**-**	**0.3**	**0.4**	**0.005**	**-**	**-**	**-**	**-**
2SD	**3.4**	**3.3**	**0.0**	**0.003**	**-**	**2.1**	**0.0**	**0.011**	**-**	**-**	**-**	**-**
20160817@323.asc	24.6	-6.1	0.2	0.078	20160805@778.asc	0.8	1.3	0.085	-	NFD	II	-
20160817@341.asc	25.7	-5.1	0.2	0.052	20160807@915.asc	-2.4	0.4	0.040	-	NFD	II	-
20160817@334.asc	28.1	-2.7	0.2	0.040	20160807@928.asc	-0.5	0.4	0.036	-	NFD	II	-
20160817@332.asc	25.8	-5.0	0.2	0.040	20160807@929.asc	0.3	0.4	0.036	-	NFD	II	-
20160817@335.asc	29.2	-1.7	0.2	0.015	20160807@932.asc	0.0	0.4	0.015	-	NFD	II	-
Avg.	**26.7**	**-4.1**	**0.2**	**0.045**	**-**	**-0.4**	**0.6**	**0.042**	**-**	**-**	**-**	**-**
2SD	**3.8**	**3.7**	**0.1**	**0.046**	**-**	**2.4**	**0.9**	**0.052**	**-**	**-**	**-**	**-**

Well C (3.343 km / 10,967 ft)

20160817@293.asc	24.5	-6.2	0.2	0.003	20160805@625.asc	0.9	0.6	0.001	-	NFD	I	Euhedral core
20160817@285.asc	24.6	-6.1	0.2	0.001	20160805@626.asc	1.4	0.6	0.000	-	NFD	I	Euhedral core
20160817@300.asc	25.8	-5.0	0.3	0.003	20160805@632.asc	0.3	0.6	0.002	-	NFD	I	Euhedral core
20160817@299.asc	25.3	-5.4	0.3	0.001	20160805@633.asc	-0.5	0.6	0.001	-	NFD	I	Euhedral core
Avg.	**25.1**	**-5.7**	**0.3**	**0.002**	**-**	**0.5**	**0.6**	**0.001**	**-**	**-**	**-**	**-**
2SD	**1.2**	**1.2**	**0.1**	**0.002**	**-**	**1.6**	**0.0**	**0.001**	**-**	**-**	**-**	**-**
20160817@287.asc	26.1	-4.7	0.2	0.003	20160805@619.asc	-0.1	0.6	0.016	-	NFD	II	-
20160817@290.asc	25.8	-5.0	0.2	0.005	20160805@620.asc	-1.5	0.6	0.004	-	NFD	II	-
20160817@288.asc	26.5	-4.3	0.2	0.031	20160805@621.asc	-1.8	0.6	0.027	-	NFD	II	-
20160817@289.asc	26.0	-4.8	0.2	0.048	20160805@622.asc	-1.0	0.6	0.034	-	NFD	II	-
20160817@286.asc	26.5	-4.3	0.2	0.016	20160805@618.asc	0.8	0.6	0.017	-	NFD	II	-
Avg.	**26.2**	**-4.6**	**0.2**	**0.020**	**-**	**-0.7**	**0.6**	**0.020**	**-**	**-**	**-**	**-**
2SD	**0.6**	**0.6**	**0.0**	**0.038**	**-**	**2.1**	**0.0**	**0.023**	**-**	**-**	**-**	**-**

Table 2.

Sample ID*	Chip #*	FIA	Host Mineral	Dol Stage	Occur[1]	Size (µm)	V/T (%)[2]	n	Tm_{ice}(°C)	Th_{LV-L}(°C)	wt. % CaCl2	wt. % NaCl	Formation Temp (°C)
C1	1	1	Cal	N/A	P	3 ~ 11	5 ~ 10	3	-35 ~ -28	71 ~ 76	16.7 ~ 33.4	0.0 ~ 8.7	77 ~ 83
C1	1	2	Cal	N/A	P	1 ~ 8	5 ~ 10	3	-35 ~ -28	76 ~ 77	16.7 ~ 33.4	0.0 ~ 8.7	82 ~ 84
C1	1	3	Cal	N/A	P	2 ~ 6	5	4	-35	62 ~ 70	23.2 ~ 32.5	0.0 ~ 4.3	67 ~ 76
C1	1	4	Cal	N/A	C	4 ~ 15	10	3	-34 ~ -28	82 ~ 92	16.7 ~ 33.4	0.0 ~ 8.7	89 ~ 101
C1	2	5	Cal	N/A	HF	3 ~ 6	5 ~ 10	5	-25	55 ~ 65	19.6 ~ 33.7	0.0 ~ 3.7	59 ~ 70
C1	2	6	Dol	II	R	1 ~ 9	10	4	-32 ~ -29	117 ~ 130	17.0 ~ 33.3	0.0 ~ 8.9	130 ~ 145
C2	1	7	Dol	IIIa	P	1 ~ 10	10	6	-24	105 ~ 113	19.6 ~ 33.8	0.0 ~ 3.7	116 ~ 125

*Sample ID and Chip # denote which chip of which replicate thick-section of Sample A, Well A (see Table 1 and Fig. 5e) was used for analysis.

1 - Occur = mode of occurrence; P = in primary crystal growth band; R = in altered (recrystallzied) domain of crystal; HF = in healed fracture; C = localized cluster;

2 - V/T = vapor / total ratio (at room temperature)

Table 3.

	Lower Bakken in ND *(shale)*	Middle Bakken in ND *(dolomitic siltstone)*	Upper Bakken in ND *(shale)*
Approx. areal extent (km^2) [(a)]	46,400	55,600	75,400
Thickness (m) [(b)]	6.6	9.9	4.7
Approx. rock volume (km^3) [(c)]	275	510	317
Porosity (volume fraction) [(d)]	0.06	0.07	0.06
Density (kg/m^3) [(e)]	2775	2710	2740
Approx. rock mass (Gt)	717	1292	816
Dolomite mass fraction (mode) [(d)]	0.045	0.135	0.045
Approx. mass dolomite (Gt)	32	174	37
Mass Mg^{2+} required for dolomitization (Gt)	**4**	**23**	**5**
Internal Mg-reservoirs:			
Compaction water volume (km^3):	511	510	589
Assumed fractional porosity reduction [(f)]	0.65	0.5	0.65
Estimate of available Mg^{2+} (Gt) [(g)]	**0.5**	**0.5**	**0.5**
Clay mineral assemblage:			
Clay mass fraction [(d)]	0.31	0.15	0.25
Mass illite-I/S clay at present (Gt) [(h)]	209	174	189
Estimated mass initial smectite clay (Gt) [(i)]	141	117	127
Estimate of available Mg^{2+} (Gt) [(j)]	**13**	**11**	**11**
Total estimate of available Mg^{2+} (Gt)	**13**	**11**	**12**
Mass Mg^{2+} available for updip export (Gt) [(k)]	9	0	7
Total mass Mg^{2+} available / required	~3	~0.5	~2.5

[(a)] *Source: LeFever (2008)*

[(b)] *Weighted average values calculated based on isopach maps of LeFever (2008)*

[(c)] *Integrated volumes determined by image-analysis of isopach maps of LeFever (2008) (ImageJ software, Schneider et al., 2012)*

[(d)] *Source: Porosity, permeability and mineralogy (XRD) dataset compiled for this study*

[(e)] *Calculated from mineralogy (XRD) dataset compiled for this study*

[(f)] *e.g., see compilation of porosity reduction curves for different lithologies in Giles (1997)*

[(g)] *Estimated here using as a guide the considerations, problem setup and calculations of Machel and Anderson (1989, pg. 907), with the assumption that the pore fluid was initially similar in composition to modern seawater.*

[(h)] *Rock mass x mass fraction clay x ratio of illite-smectite to total clay (mean value of 0.93 for the Bakken Fm.)*

[(i)] *Mass illite-I/S clay at present x molar mass smectite (402.70 g/cm^3, calculated here using examples of smectite structural formulas compiled by Chamley, 1989, pg. 13-14) / molar mass illite (389.05 g/cm^3, calculated using compositions from Table 4 of Boles and Franks, 1979).*

[(j)] *Estimated mass initial smectite clay x molar mass smectite (402.70 g/cm^3) x 1.49 mol Mg / 1 mol average smectite (compositions from Chamley, 1989, pg. 13-14) x molar mass Mg (24.305 g/mol)*

[(k)] *The quantity of Mg^{2+} in excess of the amount required to dolomitize each Bakken member.*